Monthly Notices
of the
ROYAL ASTRONOMICAL SOCIETY

Mon. Not. R. Astron. Soc. **408,** 2457–2475 (2010) doi:10.1111/j.1365-2966.2010.17302.x

Low-mass stars and brown dwarfs in Praesepe

D. E. A. Baker,[1⋆] R. F. Jameson,[1] S. L. Casewell,[1] N. Deacon,[2,3] N. Lodieu[4,5] and N. Hambly[6]

[1]*Department of Physics and Astronomy, University of Leicester, University Road, Leicester LE1 7RH*
[2]*Department of Astrophysics, Faculty of Science, Radboud University Nijmegen, PO Box 9010, 6500 GL Nijmegen, the Netherlands*
[3]*Institute for Astronomy, University of Hawaii, 2680 Woodlawn Drive, Honolulu, HI 96822, USA*
[4]*Instituto de Astrofísica de Canarias, C/ vía Lácta s/n, E-38200 La Laguna, Tenerife, Spain*
[5]*Departamento de Astrofísica, Universidad de La Laguna, E-38250 La Laguna, Tenerife, Spain*
[6]*Institute for Astronomy, SUPA (Scottish Universities Physics Alliance), University of Edinburgh, Royal Observatory, Blackford Hill, Edinburgh EH9 3HJ*

Accepted 2010 July 2. Received 2010 July 2; in original form 2010 January 29

ABSTRACT

Presented are the results of a large and deep optical–near-infrared multi-epoch survey of the Praesepe open star cluster using data from the UKIRT Infrared Deep Sky Survey (UKIDSS) Galactic Clusters Survey. Multiple colour–magnitude diagrams were used to select potential members and proper motions were used to assign levels of membership probability. From our sample, 145 objects were designated as high probability members ($p \geq 0.6$) with most of these having been found by previous surveys although 14 new cluster members are also identified. Our membership assignment is restricted to the bright sample of objects ($Z < 18$). From the fainter sample, 39 candidates were found from an examination of multiple colour–magnitude plots. Of these, two have small but significant membership probabilities. Finally, using theoretical models, cluster luminosity and mass functions were plotted with the latter being fitted with a power law of $\alpha = 1.11 \pm 0.37$ for the mass range 0.6 to 0.125 $M_{\odot}$ and an assumed cluster age of 500 Myr in the UKIDSS Z photometric band. Likewise taking an assumed cluster age of 1 Gyr we find $\alpha = 1.10 \pm 0.37$. Similar values were also found for the J and K bands. These results compare favourably with the result of Kraus & Hillenbrand ($\alpha = 1.4 \pm 0.2$) but are significantly lower than that of the more recent study conducted by Boudreault et al. ($\alpha = 1.8 \pm 0.1$).

Key words: brown dwarfs – stars: low-mass – stars: luminosity function, mass function – open clusters and associations: individual: Praesepe.

1 INTRODUCTION

Low-mass stars (LMS) and brown dwarfs (BDs) are the lowest mass objects for which the stellar formation process is applicable (Burrows et al. 2001). Locating these objects in a cluster is particularly important as it provides some of the key parameters that help define them, notably age, distance and metallicity. These can in turn be used to help provide constraints to theoretical evolutionary and atmospheric models. Another important reason for trying to locate these objects in clusters, particularly older ones, is that as the cluster ages it undergoes a process of dynamical evolution, in which the lower mass objects are preferentially ejected from the cluster into the field (de La Fuente Marcos & de La Fuente Marcos 2000). This ejection of objects causes changes to occur in the cluster's luminosity and mass function, which for a gravitationally bound association can be considered a proxy for the initial mass function (IMF) of the system. Although there have been many previous studies aimed at characterising the IMF, they have often come from many surveys conducted in different filters and with different instruments. For this reason the UKIRT Infrared Deep Sky Survey (UKIDSS) Galactic Clusters Survey (GCS; Lawrence et al. 2007) was devised. One of the clusters surveyed is the open star cluster of Praesepe.

Praesepe lies at a distance of ≈180 pc [$(M - m)_0 = 6.30 \pm 0.003$; van Leeuwen 2009] with zero reddening and near solar metallicity. Whilst the distance is fairly well constrained, there is a lack of agreement with regards to its age. Allen (1973) placed the value of Praesepe's age towards the lower end of the scale at 430 Myr and it was the standard value for many years. Later work by Vandenberg & Bridges (1984) placed it at a much higher value of 900 Myr. Their value was obtained via the fitting of models describing the main sequence to the observed colour–magnitude diagrams (CMDs). The widest range of age estimates is reported by Tsvetkov (1993) who placed a similar lower limit of 540 Myr but an upper limit of over

⋆E-mail: deab1@star.le.ac.uk

1.5 Gyr. The method of Tsvetkov does not depend on the fitting of the zero-age main-sequence but instead relied on models used to calculate the ages of δ Scuti stars that are present within the cluster. Finally, Kharchenko et al. (2005) placed the age in the middle at 795 Myr after using the Padova grid of post-main-sequence isochrones from Girardi et al. (2002). We consider this to be closest to the most likely age as there is some evidence that the Hyades cluster at 625 Myr shares a common origin with Praesepe (Eggen 1960; Henry, Anderson & Hesser 1977). However, due to the uncertainty that exists, two ages for the cluster have been adopted throughout this paper. The first is an age of 500 Myr and the second 1 Gyr. These were chosen as they coincide nicely with ages for which the NextGen (Baraffe et al. 1998) and DUSTY (Chabrier et al. 2000) theoretical models have been calculated. In this work we have used the BT-NextGen and BT-DUSTY models which are based on the aforementioned versions except they have been calculated with updated opacity data.[1]

Praesepe's members all have a common proper motion centred around $\mu_\alpha = -35.81\,\mathrm{mas\,yr^{-1}}$ and $\mu_\delta = -12.85\,\mathrm{mas\,yr^{-1}}$, again from the work by van Leeuwen based on rereduced *Hipparcos* data. This distinct proper motion allows relatively easy photometric and astrometric membership surveys to take place. The 'high-mass' stellar population ($V < 13$) was identified by Klein-Wassink (1927) with 'intermediate-mass' ($V < 17$) and 'low-mass' M dwarfs ($R > 20$) being identified by Jones & Cudworth (1983) and Hambly et al. (1995a), respectively. Further work has been carried out by Pinfield et al. (1997, 2003), Adams et al. (2002), Chappelle et al. (2005) and González-García et al. (2006). However, these surveys have often proved to be contaminated with an excess of field stars, as in the case of Adams et al. or have no proper motion information (Pinfield et al. 1997). The most comprehensive study to date was produced by Kraus & Hillenbrand (2007), who used data from the Sloan Digital Sky Survey (SDSS; York et al. 2000), Two Micron All Sky Survey (2MASS; Skrutskie et al. 2006), USNOB1.0 (Monet et al. 2003) and finally UCAC2 (Zacharias et al. 2004) to find 1010 candidate members of Praesepe, 442 being identified for the first time, down to a spectral type of around M5. The work presented in this paper is again a return to a search for this 'low-mass' population; however, we have based our search on data made available from the UKIDSS, 2MASS and SDSS.

2 THE SURVEYS

UKIDSS is a near-infrared sky survey that aims to survey some 7500 deg^2 of the northern sky within its science operation lifetime. The depth that it aims to achieve will be three magnitudes deeper than that offered by 2MASS, making UKIDSS an ideal companion to the SDSS in areas where the two coincide. UKIDSS uses the 3.8-m United Kingdom Infrared Telescope (UKIRT) located on Mauna Kea and the Wide Field Camera (WFCAM). WFCAM itself consists of four Rockwell Hawaii-II (HgCdTe) detectors, each of dimension 2048 $\times$ 2048 pixels. A single pixel represents a scale of 0.4 arcsec and the spacing between the detectors requires that four paw prints be undertaken in order to construct a single 0.8 deg^2 tile. The UKIDSS survey program consists of five separate components: The Large Area Survey, The Galactic Plane Survey, The Deep Extragalactic Survey, The Ultra Deep Survey and The Galactic Clusters Survey, which provides the focus and data for this paper.

[1] http://phoenix.ens-lyon.fr/simulator/index.faces

For more specific information on the UKIDSS programme a set of reference papers have been produced which aim to provide technical documentation on the infrared survey instrument itself (WFCAM; Casali et al. 2007), the WFCAM photometric system (Hewett et al. 2006; Hodgkin et al. 2009), the UKIDSS surveys (Lawrence et al. 2007), the pipeline processing system (Irwin et al., in preparation) and finally the science archive as described in Hambly et al. (2008).

The GCS aims to enable a comprehensive study of 10 star-forming regions and clusters, with hopes of detailing the form of the IMF and how it is affected by the environment in the substellar regime. All the data for these programmes is processed by the Cambridge Astronomical Survey Unit (CASU) and then archived and released by the WFCAM Science Archive (WSA) located in Edinburgh. Currently, UKIDSS is on Data Release 6 (DR6) as of 2009 October 13 for the ESO community (and DR3 as of the 2009 June 5 for the world release). DR6 has reported depths of $Z = 20.4$, $Y = 20.1$, $J = 19.6$, $H = 18.8$ and $K = 18.2$ (first epoch). At the time of writing the Praesepe cluster has not yet been fully surveyed with only $\approx$23 deg^2 being available in all filters and imposing a 3° radial selection from the cluster centre $\approx$18 deg^2. This can be clearly seen in Fig. 1. Because of the missing region consisting of mainly the cluster centre, a clear lack of overlap will exist between this and any of the previous bodies of work. As such, this work fails to retrieve many of the previously identified cluster members and so acts to serve as an incremental part of a full cluster survey within the UKIDSS programme.

To retrieve the data from the WSA a similar SQL query to that of Lodieu et al. (2007a) was devised (see Appendix A for the full queries). The query was adapted to cross match with the SDSS through the use of the newly implemented gcsSourceXDR7PhotoObj table. The class parameter in each of the five filter bands was set to only select objects that matched with criteria -2 or -1 in value, i.e. those that had been deemed stellar in nature by the pipeline. While this clearly limits the number of sources by requiring the object to be present in all bands, particularly at the faint end (Lodieu et al. 2007b), it does mean a greater level of reliability for the data that have been selected. Alongside the class selection criteria, the query also placed various quality control mechanisms as defined by the use of the post processing

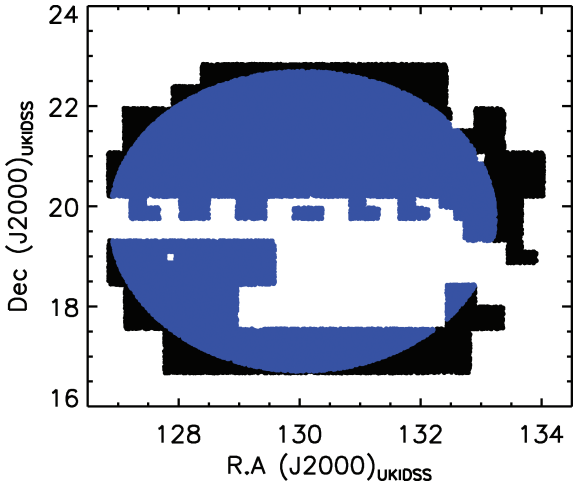

Figure 1. The full coverage of the Praesepe star cluster available from UKIDSS DR6 with the blue region denoting the sources present in the 3° radial selection.

error bits flags on the UKIDSS data and the flags contained within the SDSS subsection.[2]

The SQL query retrieved a total of 79 162 sources from the archive. When asking for the 2MASS and SDSS cross tables, the UKIDSS source identifier was used in order to merge the two separate queries into a master table, with each source containing any data from UKIDSS, 2MASS and/or SDSS. This match was performed using the TOPCAT program in the Starlink suite of programs. To try and minimize the contamination due to field stars at the outer edges of the survey area where the cluster is more diffuse we employed a radial cut of 3° from the cluster centre. This left 59 779 sources, which we call our GCS data set.

The objects found by Adams et al. (2002), Chappelle et al. (2005), Hambly et al. (1995b), González-García et al. (2006), Kraus & Hillenbrand (2007), Pinfield et al. (1997) and Pinfield et al. (2003) were then matched to this GCS data set to select only those whose survey areas overlapped and could be recovered from our data. In total 642 sources were recovered from Adams et al. (who in total report 4954 objects for their whole survey), six from Chappelle et al. (26 in total), 109 from Hambly et al. (515 in total), zero from González-García et al. (20 in total), 274 from Kraus & Hillenbrand (1130 in total) and five from each of the Pinfield surveys,[3] these can all be seen in Fig. 2.

The first run of the SQL query contained a cross-correlation between the UKIDSS DR6 GCS data set with its nearest 2MASS counterpart. This cross-correlation allows a determination of proper motion for the matched objects. Typically over a small area the astrometry provided by 2MASS is good to 50 mas (Skrutskie et al. 2006). The CASU pipeline performs its astrometric calibration for the WFCAM data based on point sources within the 2MASS catalogues. Hence, accurate relative proper motions can be derived by simply taking the difference in 2MASS and WFCAM positions and dividing by the epoch difference (Lodieu et al. 2007a; Jameson et al. 2008). This was automatically done and the results converted into mas yr^{-1} by the SQL query when run through the WSA data centre. The proper motions are described as relative as they exhibit a distinct movement in contrast to the comparably stationary background. The accuracy of the astrometry and the average time baseline of around 5 yr provides an error of ≈10 mas yr^{-1}. Of the 59 779 sources 34 990 were found to have 2MASS counterparts leaving 24 789 with no 2MASS identifier. Because 2MASS lacks the depth of UKIDSS we only retrieved the brighter of our sample ($K < 16.5$) from this data set, with the SDSS data set providing the fainter candidates. (The extent of the data set can be seen in Fig. 2.)

Thanks to the newly implemented gcsSourceXDR7PhotoObj table linking the WFCAM DR6 and SDSS DR7 data sets at the WSA, a cross-correlation between the UKIDSS data set and that of the SDSS was also available for interrogation. SDSS DR7 reported having surveyed 11 000 deg^2 in all of its five filters (*ugriz*′) which included the full area of Praesepe (Kraus & Hillenbrand 2007). Upon inspection of the survey dates it became apparent that only a short amount of time had elapsed between the survey of Praesepe by Sloan and that of UKIDSS (≈2–2.5 yr on average). The lack of a decent baseline therefore warranted a different approach in order to calculate proper motions and thus cluster membership assignment from that which will be detailed for 2MASS. Again the 59 779 UKIDSS sources were retrieved with 53 562 having an SDSS counterpart and 6253 being unique to UKIDSS. In total UKIDSS has 2225 unique sources for which no counterpart has been found in either 2MASS of SDSS (30 998 objects were present in all three surveys).

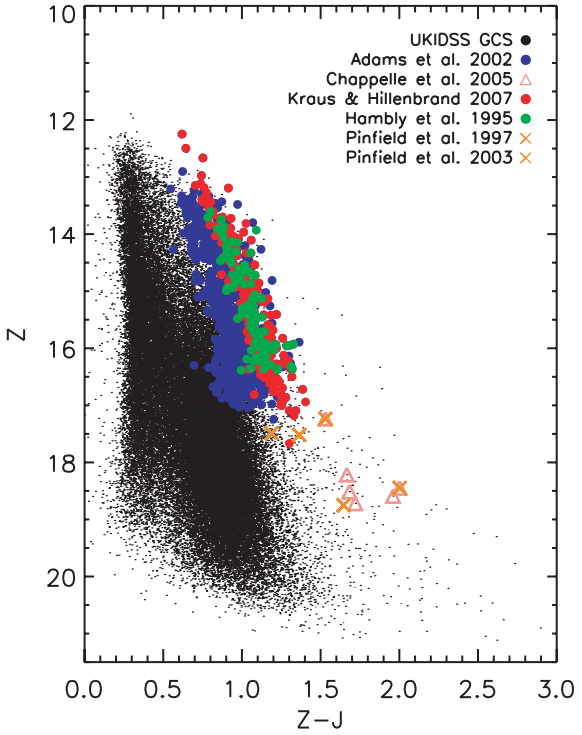

Figure 2. $(Z - J, Z)$ CMD for the ≈18 deg^2 of the Praesepe cluster selected from the WSA with a corresponding 2MASS source within the inner 3° of the cluster centre. Matches to this data set from the surveys of Adams et al. (2002), Chappelle et al. (2005), Hambly et al. (1995b), Kraus & Hillenbrand (2007) and Pinfield et al. (1997, 2003) are also shown. The survey of González-García et al. did overlap with this area; however, for those sources within the region no matches were found, due possibly to our strict selection criteria on the UKIDSS data.

3 MEMBERS OF PRAESEPE FROM 2MASS

This section will describe the processes undertaken to construct the list of candidate cluster members in Praesepe from the UKIDSS CMDs, and where possible proper motion vector point analysis based from the 2MASS–UKIDSS cross-correlation. The procedure is as follows.

(i) Select only those sources that have a 2MASS identifier associated with their UKIDSS identifier and are within 3° of the defined cluster centre (34 990 objects).

(ii) To check the proper motion errors fit the reduced data set (CMD and radius selections imposed) with a two-dimensional Gaussian, then use the σ of the Gaussian to act as a proxy for the error.

(iii) Using the theoretical isochrones, select objects that are no more than 0.3 mag to the left, and all of those on the right in both the $(Z - J, Z)$ and $(Y - K, Y)$ CMDs.

[2] The SDSS flag selections were taken from clean photometry section of the SDSS SQL query sample page http://cas.sdss.org/dr6/en/help/docs/realquery.asp. Because of the nature of the objects being investigated the constraints were placed only on bands in which the object was likely to be present i.e the *i* and *z*′ bands.

[3] The objects retrieved from the two Pinfield surveys are the same five objects.

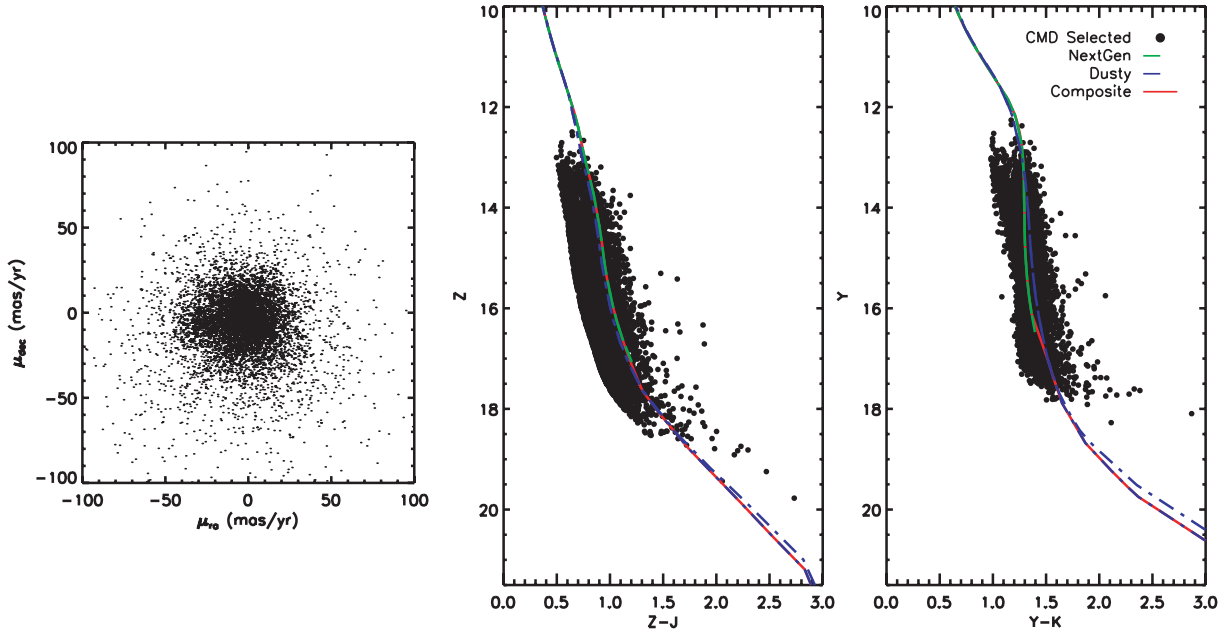

Figure 3. On the left is the VPD for the sources selected from our spatial and colour cuts in the $(Z-J, Z)$ and $(Y-K, Y)$ CMD as shown in the middle and on the right, respectively. The cluster can be seen as the overdensity of objects around -30 and -10 mas yr^{-1} in right ascension and declination. The green dashed line is the theoretical isochrone for the BT-NextGen evolutionary model and the blue the BT-DUSTY equivalent. Both the 500 Myr and 1 Gyr flavours have been considered due to the uncertainty in the age of Praesepe.

(iv) Analyse the resulting vector point diagram (VPD) for this colour selected data set across a range of magnitude bins and inferring from the probability fitting routine a level of cluster membership for each object. Then selecting out a high probability sample (HPM) as those objects with assigned probabilities $p \geq 0.60$.

(v) Again look at this HPM sample and reject any obvious non-photometric candidates.

3.1 Calculating proper motions

The cross-correlation of UKIDSS with 2MASS provided a value for the matched objects proper motion in $\mu_\alpha \cos_\delta$ and μ_δ. An estimate of the errors based on the time baseline and specifications of 2MASS is $\approx$10 mas yr^{-1}. To confirm this error estimate, the proper motions for those sources that lay within 3° of the cluster centre (which were spread over a region of proper motion space from -150 to 150 mas yr^{-1}) were divided into bins of 20 mas yr^{-1} and the number in each bin totalled. A two-dimensional Gaussian was then fitted enabling, a determination of the cluster spread. Objects that were defined as being outside of the 3σ limit were then removed and the fit reapplied. The σ of the Gaussian then provides an estimate for the error in the proper motions (Jameson et al. 2008) and was found to be of the order of $\approx$12 mas yr^{-1}, instead of our assumed 10 mas yr^{-1}.

3.2 Colour–magnitude diagrams

In order to select candidates from the CMDs we made use of the BT-NextGen and BT-DUSTY theoretical isochrones which have had the distance modulus of the cluster added to them in order. The models represent different evolutionary paths for describing objects with and without 'dusty' atmospheres. Because of the temperatures and masses being explored by this survey the objects involved inhabit both of these regimes and so the two isochrones need to be combined. To create a composite isochrone line, the data points from the BT-NextGen isochrone in the relevant band filter were taken to their minimum temperature $\approx$3000 K. This temperature lies just above where dust grains begin to form in the BD atmosphere and the BT-NextGen models become invalid. We thus combine the BT-DUSTY isochrone models ($T_{\rm eff} < 3000$ K) with the BT-Nextgen models at this point with a simple straight line added in between the resulting break. This composite isochrone was calculated for both the 500 Myr and 1 Gyr evolutionary models due to the uncertainty in the age of Praesepe. It was then employed in both the $(Z-J, Z)$ and $(Y-K, Y)$ CMDs with sources lying no more than 0.3 mag to the left in the horizontal direction from the line and those to the right being selected and passed to the proper motion fitting routine. See Fig. 3 for the VPD and the two CMDs associated with the spatial and colour cut selections. This process selected 7127 objects out of the possible 34 990. This selection is rather conservative as it aimed to include all the cluster members from the previous surveys, most notably that of Adams et al. (2002) whose objects appear far bluer than those found by both Kraus & Hillenbrand (2007) and by Hambly et al. (1995b).

4 CLUSTER DISTRIBUTIONS AND MEMBERSHIP PROBABILITY

To calculate the membership probabilities for the data sample two distributions were fitted to the cluster. One, a circularly symmetric Gaussian as originally employed by Sanders (1971) and also Francic (1989), and two, an exponential decaying in the direction of the cluster proper motion centre coupled with a perpendicularly oriented Gaussian (Hambly et al. 1995b; Deacon & Hambly 2004). For the fitting process to work the cluster proper motion centre $(-35.81, -12.85)$ is rotated from its original position on the VPD to lie on the y-axis. The following set of equations describe the field distribution ($\Phi_{\rm f}$), cluster distribution ($\Phi_{\rm c}$) and the normalization to

Table 1. Fitted parameter values for the set of magnitude bins analysed by the VPD-probability fitting routine.

Interval	f	σ	μ_{xc}	μ_{yc}	τ	Σ_x	μ_{xf}
$12.00 < Z < 14.00$	0.75	3.28	3.53	27.73	21.46	18.94	−5.43
$14.00 < Z < 16.00$	0.71	5.45	4.43	30.65	14.26	18.89	−4.00
$16.00 < Z < 18.00$	0.89	5.43	−0.27	31.87	14.91	19.54	−1.95

the exponential (c_o):

$$\Phi_f = \frac{c_o}{\sqrt{2\pi}\Sigma_x}\exp\left(-\frac{(\mu_x-\mu_{xf})^2}{2\Sigma_x^2}-\frac{\mu_y}{\tau}\right), \quad (1)$$

$$\Phi_c = \frac{1}{2\pi\sigma^2}\exp\left(-\frac{(\mu_x-\mu_{xc})^2+(\mu_y-\mu_{yc})^2}{2\sigma^2}\right), \quad (2)$$

$$c_o = \frac{1}{\tau(e^{-(\mu_1/\tau)}-e^{-(\mu_2/\tau)})}, \quad (3)$$

where

$$c_o\int_{\mu_1}^{\mu_2} e^{-(\mu_y/\tau)}d\mu_y = 1. \quad (4)$$

The values of μ_x and μ_y refer to the proper motion attributed to each individual object. The quantity σ is the Gaussian width, whilst μ_{xc} and μ_{yc} are the cluster's mean proper motion. Σ_x is the proper motion dispersion value in x and τ the exponential scalelength for the field proper motion distribution in y. μ_{xf} is the field mean proper motion in x and finally μ_1 and μ_2 are the limits for the normalization to the exponential c_o. For the rotated VPD these were set at 20 and 70 mas yr^{-1} to avoid the mass of stars centred around (0, 0).

Combining the field star distribution and the cluster distribution with information about the fraction of stars which are field stars (f) the resulting expression for the total distribution (Φ) is

$$\Phi = f\Phi_f + (1-f)\Phi_c. \quad (5)$$

After employing the method of maximum likelihood with Θ representing one of the free parameters,

$$\sum_i \frac{\delta \ln\Phi_i}{\delta\Theta} = 0, \quad (6)$$

a set of non-linear equations can be defined as the following:

$$f : \sum_i \frac{\Phi_f-\Phi_c}{\Phi} = 0, \quad (7)$$

$$\sigma : \sum_i \frac{\Phi_c}{\Phi}\left(\frac{(\mu_x-\mu_{xc})^2+(\mu_y-\mu_{yc})^2}{\sigma^2}-2\right) = 0, \quad (8)$$

$$\Sigma_x : \sum_i \frac{\Phi_f}{\Phi}\left(\frac{(\mu_x-\mu_{xf})^2}{\Sigma_x^2}-1\right) = 0, \quad (9)$$

$$\mu_{xf} : \sum_i \frac{\Phi_f}{\Phi}(\mu_x-\mu_{xf}) = 0, \quad (10)$$

$$\mu_{xc} : \sum_i \frac{\Phi_c}{\Phi}(\mu_x-\mu_{xc}) = 0, \quad (11)$$

$$\mu_{yc} : \sum_i \frac{\Phi_c}{\Phi}(\mu_y-\mu_{yc}) = 0, \quad (12)$$

$$\tau : \sum_i \frac{\Phi_f}{\Phi}\left(\frac{\mu_y}{\tau}-1-c_o(\mu_1 e^{-(\mu_1/\tau)}-\mu_2 e^{-(\mu_2/\tau)})\right) = 0. \quad (13)$$

To each of these equations a bisection algorithm was devised that checks for root bracketing and then proceeds to find the root to the desired level of accuracy. Once one parameter has been fitted, the next parameter is subject to the same process. Finally once τ has been found the process reverts back to its starting point and runs again until all the free parameters have been fixed (showing no further sign of deviation). To start the process a set of initial values is required for the free parameters, these are as in Deacon & Hambly (2004). Once the values are fixed the membership probabilities for the ith object can be calculated thus

$$p_i = \frac{(1-f)\Phi_{ci}}{\Phi_i}. \quad (14)$$

The fitted values for each magnitude interval are shown in Table 1 and VPDs and probability histograms in Fig. 4. Taking the sigma value of the Gaussian from Section 3.1 and placing it over the cluster's centre of proper motion we find 380 objects with a probability assignment. Of these, 121 have probabilities that place them in the high-membership bracket ($p > 0.60$). In total 145 sources are found

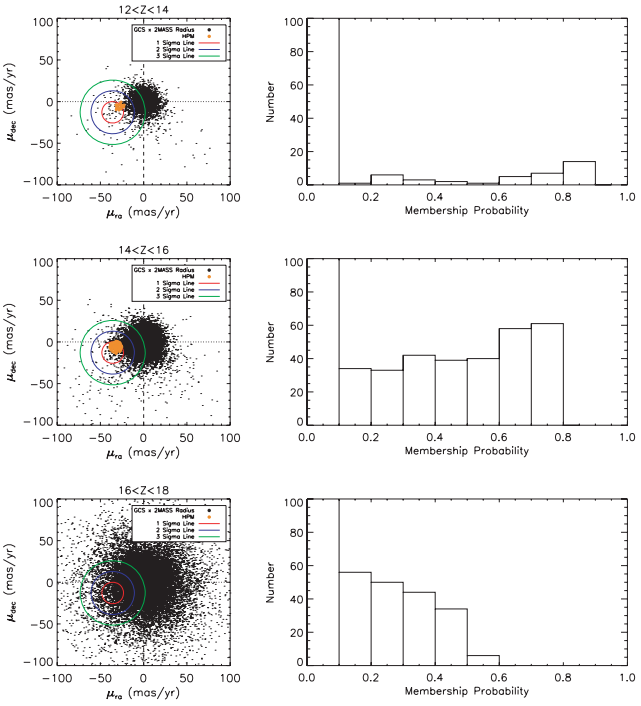

Figure 4. Proper motion VPDs and the resulting probability histograms for each magnitude interval in the probability fitting of the Praesepe data. In each plot the three coloured lines represent the 1σ, 2σ and 3σ errors obtained from our estimate of proper motion errors by way of the 2D Gaussian fit, they have been shifted to be located over the clusters proper motion centre. The points in orange show our HPM.

to have a $p \geq 0.60$. The 24 lying outside the sigma selection are still very much consistent with the cluster as can be seen by small spread of objects proper motion space in Fig. 4.

5 MEMBERS OF PRAESEPE FROM SDSS

In this section the process for locating any possible candidates/members of the Praesepe cluster from available data within the cross link between UKIDSS and SDSS will be described.

(i) Select those objects that are again within the 3° radial cut from the cluster centre. These objects are only present in UKIDSS–SDSS data set. Any corresponding SDSS–2MASS source would have been treated within the previous section.

(ii) Select the list of candidate objects from six CMDs.

(iii) Extract the FITS files for these objects from the WSA and SDSS data access server.

(iv) Calculate a pixel to pixel transformation between the two images and using the epoch difference calculate a proper motion.

(v) Perform a basic probability analysis on the resulting data.

5.1 Extracting the candidates

Performing the same radial cut with objects only present in the UKIDSS–SDSS match (no 2MASS counterpart) led to a selection of 22 564 objects. To extract the candidates from this list, a series of photometric cuts were applied in a range of different CMDs. These can be seen in Fig. 5. These CMDs made use of a range of different filters and known locations of LMS/VLMS and BDs as detailed by Hawley et al. (2002). Objects within these predefined regions were selected for further analysis.

5.2 Refinement of proper motions

The primary problem with the SDSS data set is the small epoch difference between the two surveys which subsequently results in large errors on the proper motion. This, coupled with a small number of objects (<100) means that the analysis as performed for the 2MASS data is not applicable. An alternate approach has therefore been taken in order to assign membership probabilities to these candidates. To begin with, suitable queries were developed to allow the acquisition of the catalogue and FITS flat files from each survey's data centre.[4] The candidate object were then located and a set of reference objects selected. These reference objects had to be common to both chips (appearing in each epoch), be in the magnitude range $12.0 < Z < 18.0$, have ellipticities less than 0.2 (from UKIDSS catalogue data) and not sit within 5 per cent of the chip border (in pixels) in order to help minimize any radial distortion effects.

The list of reference objects are used to create a 12 parameter transformation (where too few reference objects were present for the quadratic fit a linear six parameter fit was tried instead) that allows the motion of the candidate object between the two epochs to be calculated. Reference objects that are shown to be moving at a rate greater than three times the rms value of the fit are discarded. The revised reference list is again passed to the fitting routines in order to calculate the correct coefficients that describe the motion between the two epochs. This motion is then converted into mas yr^{-1} through the use of the following equations:

$$\mu_\alpha = \frac{((\mathrm{CD1\_1} \times \Delta x + \Delta y \times \mathrm{CD1\_2}) \times 3600 \times 1000)}{\mathrm{epoch\_difference}}, \quad (15)$$

$$\mu_\delta = \frac{((\mathrm{CD2\_1} \times \Delta x + \Delta y \times \mathrm{CD2\_2}) \times 3600 \times 1000)}{\mathrm{epoch\_difference}}. \quad (16)$$

The quantities CD1_1, CD1_2, CD2_1 and CD2_2 are the world coordinate transformation matrix elements contained within the FITS header (Greisen & Calabretta 2002), whilst Δx and Δy simply refer to the change in pixel elements. The direction in μ_α is finally further corrected by multiplying by the appropriate $\cos\delta$ value.

In order to calculate errors, the magnitudes of all possible objects were calculated on the reference image frames using the relevant calculations listed on the SDSS[5] and WSA[6] pages. The x and y pixel centroiding errors reported for each object in the catalogue files were then totalled for each bin of width 2 mag and divided by the number in that magnitude bin to give an average centroiding uncertainty value. These values were then added in quadrature with the rms in that particular direction as found by the 12 parameter quadratic fit:

$$\mathrm{error\_pm} = \sqrt{\mathrm{rms}^2 + \mathrm{err}^2_{\mathrm{epoch1}} + \mathrm{err}^2_{\mathrm{epoch2}}}. \quad (17)$$

The values representing the error found in the x or y direction for both epoch 1 and epoch 2 measurements are in turn calculated from the following:

$$\mu_\alpha\mathrm{\_err} = \frac{((\mathrm{CD1\_1} \times x\mathrm{err} + y\mathrm{err} \times \mathrm{CD1\_2}) \times 3600 \times 1000)}{\mathrm{epoch\_difference}}, \quad (18)$$

$$\mu_\delta\mathrm{\_err} = \frac{((\mathrm{CD2\_1} \times x\mathrm{err} + y\mathrm{err} \times \mathrm{CD2\_2}) \times 3600 \times 1000)}{\mathrm{epoch\_difference}}, \quad (19)$$

where $x$err and $y$err represent the centroiding errors in the x and y directions as described in the previous paragraph. The errors on the proper motion are likely an overestimation of the astrometric errors as they are based on the rms from the fitting process rather than an error in the transformed coordinate.

To try and calculate membership probabilities for these objects, an attempt at using control data to determine levels of contamination was undertaken.The cluster circle and two control circles of radius 26 arcsec were used. The radius value is the average value taken from the 12 parameter fit information, ignoring any obvious discrepancies (as objects become fainter the centroiding errors become larger). Those that were in the faintest magnitude bin had centroiding errors a factor ten larger than for the other candidates and so were discounted from the average). The circles were located at the same distance from (0,0) in proper motion space and as is usual, the data were split into magnitude bins with the probability being calculated using equation (20):

$$P_{\mathrm{membership}} = \frac{N_{\mathrm{cluster}} - N_{\mathrm{control}}}{N_{\mathrm{cluster}}}. \quad (20)$$

$P_{\mathrm{membership}}$ is the probability assigned for a particular magnitude bin, N_{cluster} the number of field and cluster stars within the cluster

[4] For the SDSS data this involved creating a few specific requests as the catalogue data are split amongst a wide range of files. The SDSS DAS has also recently been updated to SDSS DAS version 2 for use with DR7, users are instructed to read the DR7 release website for more information.

[5] SDSS magnitude algorithm calculations: http://www.sdss.org/dr6/algorithms/fluxcal.html#counts2mag

[6] WFCAM magnitude algorithm calculations: http://surveys.roe.ac.uk/wsa/flatFiles.html#catmags

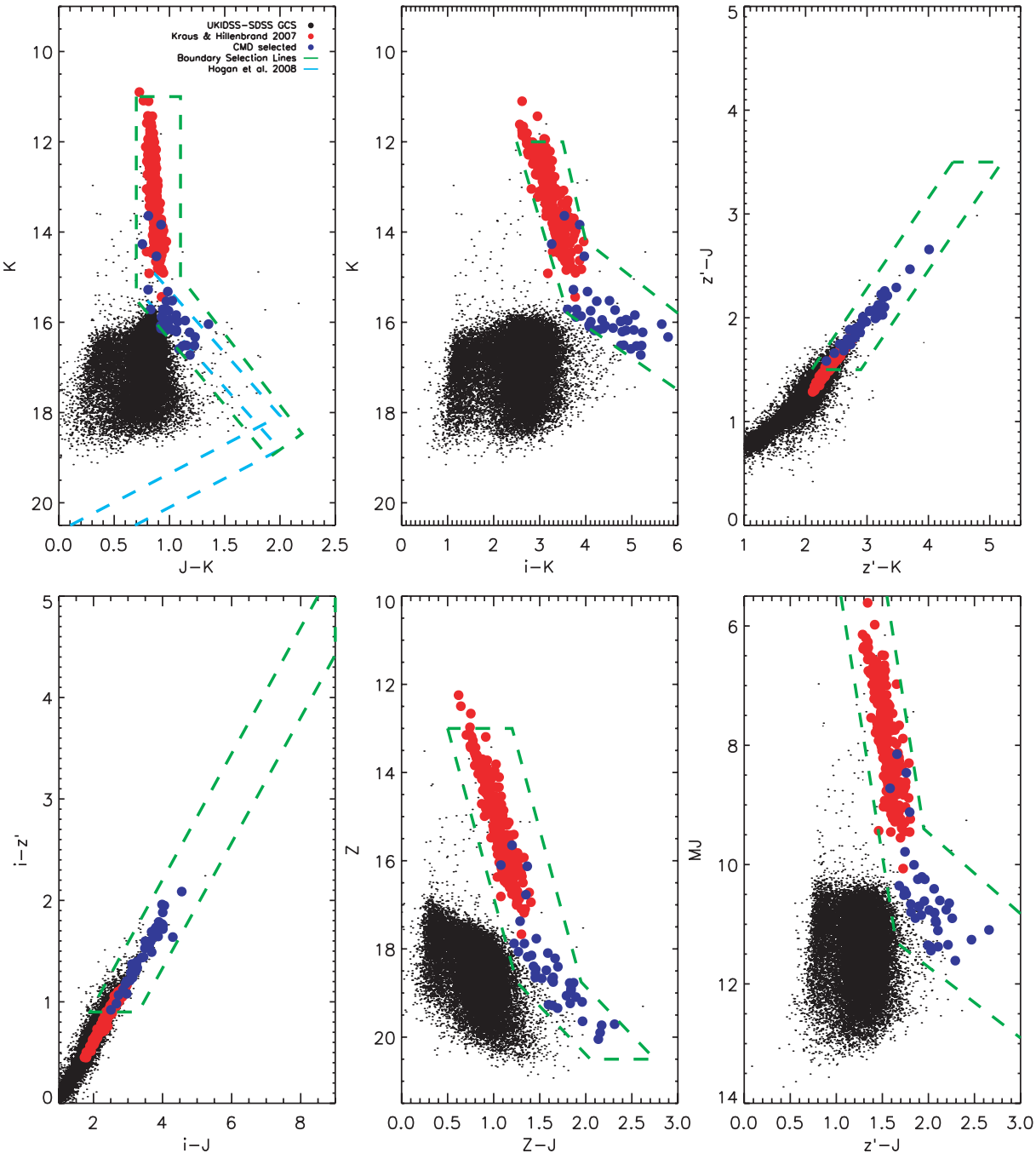

Figure 5. CMDs for SDSS and UKIDSS photometric bands showing the selection regions (as denoted by the green dashed lines) used to extract the set of 39 candidate objects as shown by the blue circles. The objects of Kraus & Hillenbrand (2007) shown in red have been used alongside information from plots in fig. 9 of Hawley et al. (2002) to denote the appropriate regions for the cluster sequence. Additionally the cluster sequence for the Hyades (a cluster of similar age to Praesepe) as found by Hogan et al. (2008) has been corrected for the distance of Praesepe and over plotted in the $J - K, K$ plot (blue dashed line) to help trace any possible cluster sequence. The black dots are the UKIDSS–SDSS sources that are not present in the UKIDSS–2MASS population.

circle and $N_{\rm control}$ the number of field stars. Thus $N_{\rm cluster} - N_{\rm control}$ should give the number of Praesepe members. One flaw to this method as reported by Casewell et al. (2007) is that this method is dependent on the chosen location of the control circle. A solution to correct this is to use the field star count within the annulus of Fig. 6 and scale this to the area of the cluster circle to estimate levels of contamination. The resulting probabilities for the control circles and annulus are reported in Table 2. Any negative probabilities have been altered to 0.00. The only magnitude bin to contain a positive probability is the bin $19 < Z \leq 20$, for which the control data revealed a probability of 0.5 and 1.0. The annulus method for the same magnitude bin put the probability at 0.58. These membership probabilities should be viewed with caution as the low numbers (i.e. few objects) make the probabilities difficult to fully substantiate. As such, objects in these fainter magnitude bins have not been taking into consideration when constructing the luminosity and mass functions reported in Section 6. When the survey of the cluster centre is complete it is hoped that not only will more LMS/BD

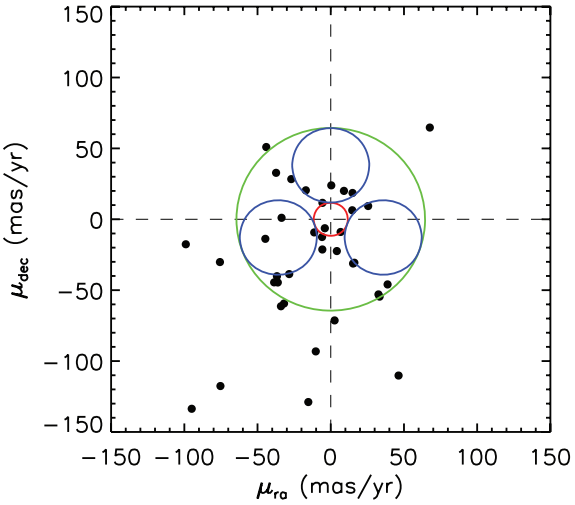

Figure 6. Proper motion vector diagram for the 39 UKIDSS–SDSS candidate objects selected from the photometric cuts. The cluster location is at $\mu_\alpha = -35.81\,\mathrm{mas\,yr^{-1}}$ & $\mu_\delta = -12.85\,\mathrm{mas\,yr^{-1}}$ with the two control circles and the annulus used for the second measure of probability also plotted. None of these objects are included in the luminosity and mass function analysis.

candidates be found but that the increase in numbers will also allow for a more robust membership probability to be assigned.

6 CLUSTER MASS AND LUMINOSITY FUNCTIONS

In order to produce the luminosity function of the cluster the effects of incompleteness on the data must be taken into account. As magnitude increases, the number of objects in a specified magnitude bin of uniform distribution will also increase. Counting the number of stars present and comparing it to this predicted rate of growth will show up any signs of incompleteness. This is done by taking the logarithm of the number of stars in the magnitude bin and fitting a best-fitting line to the data up until this 'drop off' point. An estimate for the level of incompleteness is calculated from the deficit. For the purposes of this study the best-fitting line was fitted between the black points in Fig. 7 for the UKIDSS–2MASS data set in the Z, J and K filters. The drop off can be clearly seen at the fainter magnitudes with the brighter magnitude drop off likely caused by bright cut-off limit of the surveys.

The cluster luminosity function (Fig. 8) was calculated by summing the assigned membership probabilities of each object in bins of width one magnitude. Each interval was then multiplied by the incompleteness factor, producing the correction from the dashed blue to solid black lines. In order to avoid distorting the luminosity function we applied this process to the UKIDSS–2MASS population only. The fainter magnitudes and tentative membership probabilities of the UKIDSS–SDSS candidates excluded them, as inappropriately large correction factors would have to be applied. The luminosity function can be seen to have a clear and well defined peak in each of the filters followed by a decrease due to a change in slope of the mass–luminosity relationship. The first point in the J-band luminosity function has been artificially raised due to an large incompleteness factor being applied. This point is thus not treated when fitting the mass function. The errors shown are simply Poisson errors.

To convert the cluster luminosity function into a mass function a mass–luminosity relationship is required (see Fig. 9). Again a combined relationship formed from the BT-NextGen and BT-DUSTY models was constructed. Cubic spline interpolation was used to interpolate between the points. As the age of the Praesepe cluster is not well confined, this mass–luminosity relationship has again been constructed based of both the 500 Myr and 1 Gyr model data.

If one considers a magnitude interval of width dM the total number of stars (dN) will be given by

$$\mathrm{d}N = \Phi(M)\,\mathrm{d}M, \tag{21}$$

where $\Phi(M)$ is the luminosity function. In the corresponding mass interval the same dN is now given by $\xi(m)\,\mathrm{d}\,m$, where dm is the interval in the mass range and $\xi(m)$ is the mass function.

Hence to calculate the mass function the previous equations can be easily rearranged to the form of

$$\xi(m) = \frac{\Phi(M)\,\mathrm{d}M}{\mathrm{d}m}. \tag{22}$$

In Fig. 10, Praesepe's cluster mass function is plotted with a single power-law fit for the points between 0.6 and 0.125 $\mathrm{M}_\odot$ for the Z photometric band. The J and K bands have been treated similarly but due to the corrections applied for the incompleteness affecting a wider range of magnitudes a narrower mass range was considered. The form of the power law is shown below:

$$\xi(m) \propto m^{-\alpha}. \tag{23}$$

The results of this fitting are that $\alpha_{500\,\mathrm{Myr}} = 1.11 \pm 0.37$ and $\alpha_{1\,\mathrm{Gyr}} = 1.10 \pm 0.37$. For the J and K bands the results were $\alpha_{500\,\mathrm{Myr}} = 1.07, \alpha_{1\,\mathrm{Gyr}} = 1.07$ and $\alpha_{500\,\mathrm{Myr}} = 1.09, \alpha_{1\,\mathrm{Gyr}} = 1.09$, respectively. These values are much lower than the Salpeter IMF (2.35) but the upper limits agree roughly with the values calculated and cited by Kraus & Hillenbrand (2007) of $\alpha = 1.4 \pm 0.2$. The Kraus & Hillenbrand result was derived using a mass–spectral type relationship; however, after retrieving 2MASS J-band photometry for their objects and constructing the J -band luminosity function as

Table 2. Probability of membership, magnitude range for our methods of calculating probabilities of membership using the annulus as well as the two control areas.

Magnitude range	Probability annulus	Probability $\mu_\alpha = 0\,\mathrm{mas\,yr^{-1}}$ $\mu_\delta = +37.85\,\mathrm{mas\,yr^{-1}}$	Probability $\mu_\alpha = +35.66\,\mathrm{mas\,yr^{-1}}$ $\mu_\delta = -12.70\,\mathrm{mas\,yr^{-1}}$
$15 < Z < 16$	0.000	0.000	0.000
$16 < Z < 17$	0.000	0.000	0.000
$17 < Z < 18$	0.000	0.000	0.000
$18 < Z < 19$	0.000	1.000	0.000
$19 < Z < 20$	0.581	0.500	1.000
$20 < Z < 21$	0.000	0.000	0.000

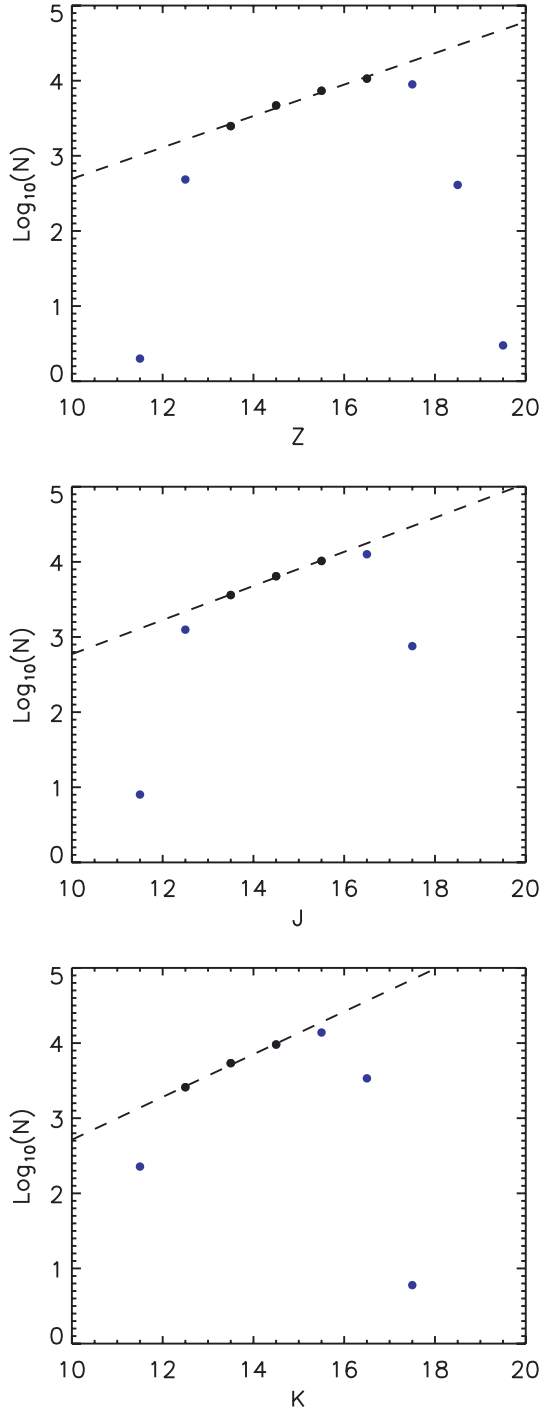

Figure 7. An estimate of the incompleteness in the 2MASS selected Praesepe data set for the UKIDSS Z, J and K bands, respectively. The black dotted line is a least squares fit to the associated black points in figure. There is clearly a drop off at the end of the functions whilst the deficit for the brightest magnitude bins is caused by saturation effects.

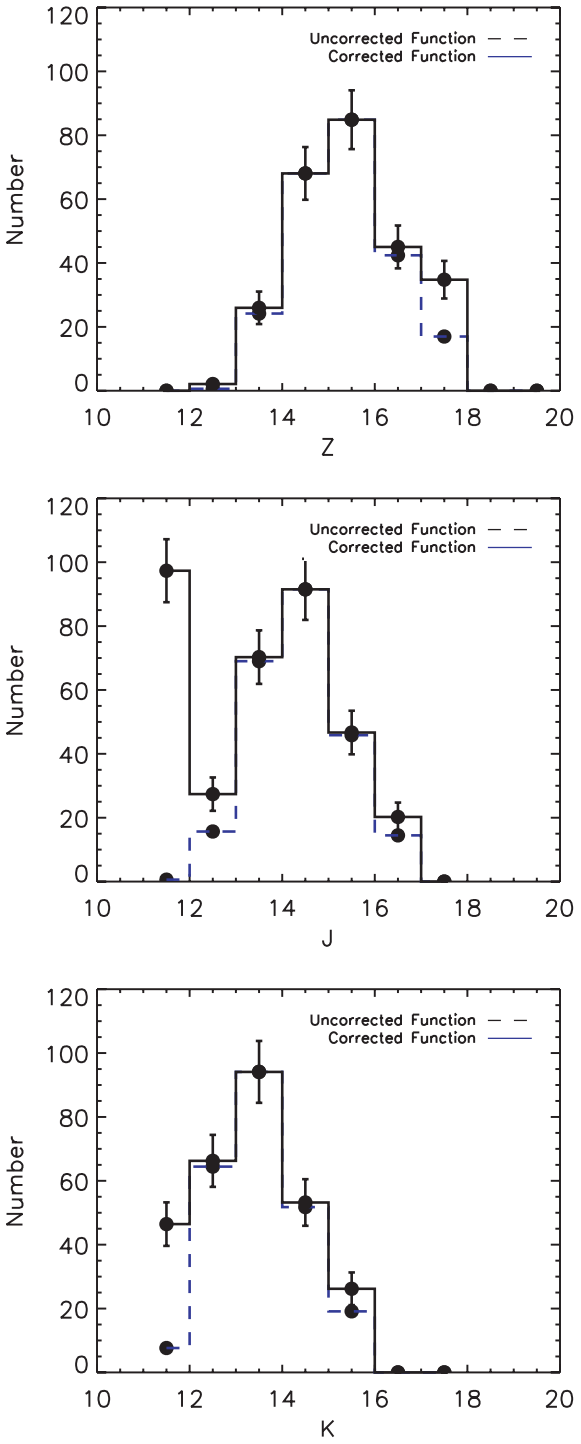

Figure 8. The luminosity functions derived for the Praesepe star cluster in the Z, J and K bands. The distribution rises to a peak before starting to decay due to the change in the slope of the mass–luminosity relationship. The error bars are Poisson errors.

we have done for our UKIDSS–2MASS sample we find α to differ by only 0.1.

A more recent survey of the cluster centre has also just been carried out by Boudreault et al. (2010). The authors identify some 150 candidate members with six expected to be BDs. Of these six only three are currently within our survey region, objects 55, 909 and 910. Objects 55 and 909 are precluded from our search due to their morphological classification in the UKIDSS data. Object 910 is present and photometrically appears to agree with Boudreault et al. ($J = 17.66, K = 16.8$). The presence of other photometric bands has, however, shown this object to be far too blue in the $Z - J, J$ diagram ($Z = 18.33$) for it to be considered as a cluster member by our current analysis. The value presented by Boudreault et al. of $\alpha = 1.8 \pm 0.1$ for $\xi(m)$ (the mass function) appears to be much

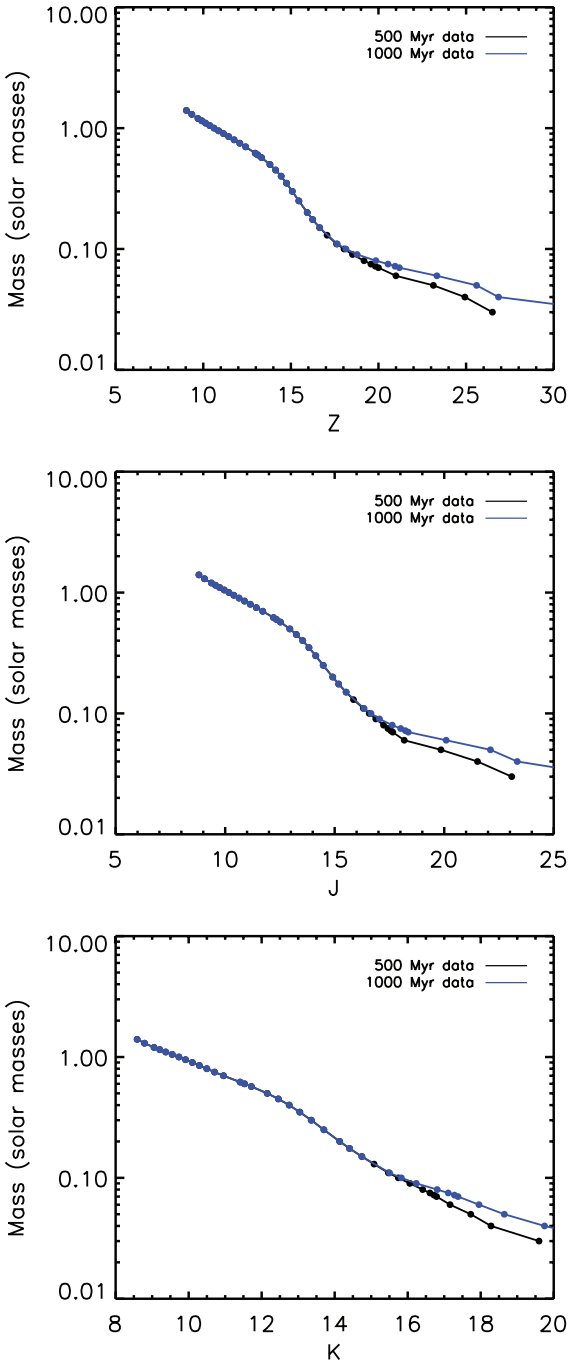

Figure 9. The mass–luminosity relationship used in this study is based off a composite BT-NextGen and BT-DUSTY line with a cubic spline interpolation. The black points represent the 500-Myr data whilst the blue the 1-Gyr data. The lines only start to deviate appreciably at faint magnitudes, which we do not investigate. Shown here is the mass–luminosity relationship for the Z, J and K bands, respectively.

greater than our calculated value and more in line with the upper value presented by Kraus & Hillenbrand. The survey, however, does not use proper motion information and restricts its objects to candidates with uniform probability of membership ($p = 1.0$). Obtaining the J -band photometry of the 150 Boudreault et al. objects and treating them in the same manner again with our luminosity–mass relationship confirms their result as we find $\alpha = 1.85 \pm 0.15$. See Table 3 for a summary of the results. It is important then that a full

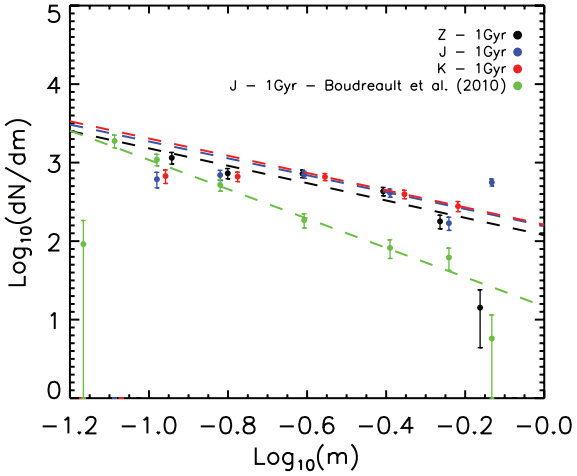

Figure 10. The derived cluster mass function with the power-law fit for the Z photometric band shown in dashed black. The FITS for the J and K bands are also shown in blue and red, respectively. The green points are taken from Boudreault et al. (2010). The error bars are Poisson errors. For clarity only the 1-Gyr data and fit has been plotted as there is little deviation between that and the 500-Myr fit.

Table 3. Mass function results from previous surveys.

Survey	Passband	Mass range ($M_\odot$)	Slope
Baker et al.	Z	0.125–0.6	1.10 ± 0.37
Baker et al.	J	0.20–0.5	1.07
Baker et al.	K	0.20–0.5	1.09
Kraus and Hillenbrand	SED[a]	0.17–1	1.4 ± 0.2
Boudreault et al.	J	0.10–0.7	2.3 ± 0.2
Boudreault et al.	J	0.18–0.45	1.8 ± 0.1

[a]See the appendix of Kraus & Hillenbrand (2007) for a discussion on how the multiple photometric bands coupled with theoretical models were used to derive masses for each spectral type.

survey including the more densely populated centre takes place as this would likely increase the number of members found (particularly at the lower mass end) thus altering the IMF that would be observed. The full extent of this change is of course unknown. It is clear, however, that even with a more complete data set there are likely to be few BDs within the Praesepe cluster. This is consistent with a cluster of such age having undergone many cycles of equipartition of energy, so ejecting low-mass objects from the cluster. The true record breakers in the low-mass stakes will therefore be found as companions to other objects as the combined system mass would restrict the amount ejected through dynamical events.

7 SUMMARY

A study of available UKIDSS data on the Praesepe star cluster combined with archive data from the 2MASS and SDSS surveys for the range of $12 \leq Z < 21$ has found, through a combination of proper motion and CMD selections 145 HPM (see Fig. 11 and Appendix B), of which, 14 appear to be new members, Appendix C. The majority of the detected HPM objects have also been found in more than one previous body of work, almost certainly confirming their status as cluster members. These objects all inhabit a fairly bright magnitude region on the cluster sequence as they have been derived from investigation of the brighter UKIDSS–2MASS data set. The

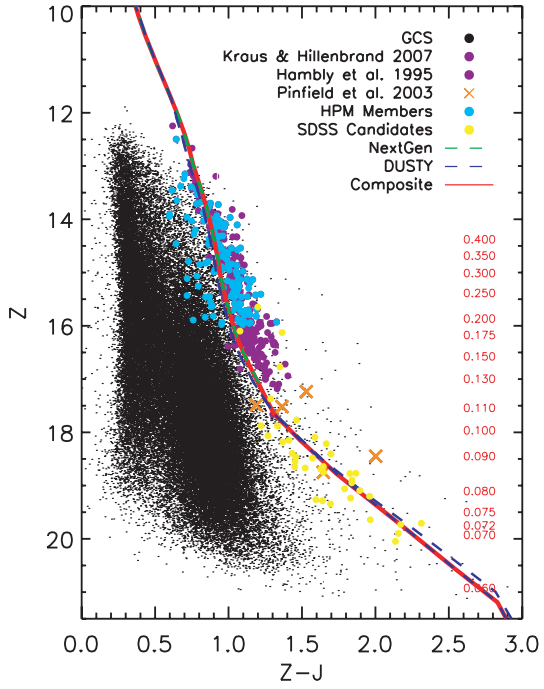

Figure 11. A $Z-J, Z$ CMD showing the cluster members given by Hambly et al. and Kraus & Hillenbrand alongside the 145 HPM derived from this work. The BT–NextGen, BT–DUSTY and composite selection lines are also shown as are the masses (in units of solar mass) given by those models for the 500 Myr case. The candidate UKIDSS–SDSS members are also shown to show the limits of the survey. Most of the UKIDSS–SDSS objects were found in this analysis to be non-members.

UKIDSS–SDSS data set, whilst allowing fainter objects to be examined, suffers from a short time base between observations and small number statistics making membership assignments difficult to quantify (see Appendix D for a list of the candidate objects). An investigation into the cluster luminosity and hence mass function was also carried out. The upper limits of the latter agree with a previous result given by Kraus & Hillenbrand (2007), confirming that although a low-mass population of objects may have existed the dynamical evolution of the cluster over its lifetime has led to a significant population depletion. Only when a full survey of the cluster with UKIDSS is complete and second epoch K data available can one hope to truly evaluate this cluster.

ACKNOWLEDGMENTS

DEAB acknowledges the support of an STFC Postgraduate studentship. NL was supported by the Ramón y Cajal fellowship number 08-303-01-02. This publication makes use of data products from the United Kingdom Infrared Deep Sky Survey, the Sloan Digital Sky Survey, the 2MASS, the SIMBAD data base, operated at CDS, Strasbourg, France and NASA's Astrophyics Data System Bibliographic Services. The SDSS is managed by the Astrophysical Research Consortium (ARC) for the Participating Institutions. The Participating Institutions are The University of Chicago, Fermilab, the Institute for Advanced Study, the Japan Participation Group, The Johns Hopkins University, Los Alamos National Laboratory, the Max-Planck-Institute for Astronomy (MPIA), the Max-Planck-Institute for Astrophysics (MPA), New Mexico State University, University of Pittsburgh, Princeton University, the United States Naval Observatory and the University of Washington. Funding for the Sloan Digital Sky Survey (SDSS) has been provided by the Alfred P. Sloan Foundation, the Participating Institutions, the National Aeronautics and Space Administration, the National Science Foundation, the US Department of Energy, the Japanese Monbukagakusho and the Max Planck Society. The SDSS Web site is http://www.sdss.org/. The Two Micron All Sky Survey is a joint project of the University of Massachusetts and the Infrared Processing and Analysis Center/California Institute of Technology, funded by the National Aeronautics and Space Administration and the National Science Foundation. The authors would like to thank France Allard for the use of the Phoenix web simulator at http://phoenix.ens-lyon.fr/simulator/index.faces which has been used in this research.

REFERENCES

Adams J. D., Stauffer J. R., Skrutskie M. F., Monet D. G., Portegies Zwart S. F., Janes K. A., Beichman C. A., 2002, AJ, 124, 1570
Allen C. W., 1973, Astrophysical Quantities. Athlone Press, London
Baraffe I., Chabrier G., Allard F., Hauschildt P. H., 1998, A&A, 337, 403
Boudreault S., Bailer-Jones C. A. L., Goldman B., Henning T., Caballero J. A., 2010, A&A, 510, A27
Burrows A., Hubbard W. B., Lunine J. I., Liebert J., 2001, Rev. Modern Phys., 73, 719
Casali M. et al., 2007, A&A, 467, 777
Casewell S. L., Dobbie P. D., Hodgkin S. T., Moraux E., Jameson R. F., Hambly N. C., Irwin J., Lodieu N., 2007, MNRAS, 378, 1131
Chabrier G., Baraffe I., Allard F., Hauschildt P., 2000, ApJ, 542, 464
Chappelle R. J., Pinfield D. J., Steele I. A., Dobbie P. D., Magazzù A., 2005, MNRAS, 361, 1323
Deacon N. R., Hambly N. C., 2004, A&A, 416, 125
de La Fuente Marcos R., de La Fuente Marcos C., 2000, Ap&SS, 271, 127
Eggen O. J., 1960, MNRAS, 120, 540
Francic S. P., 1989, AJ, 98, 888
Girardi L., Bertelli G., Bressan A., Chiosi C., Groenewegen M. A. T., Marigo P., Salasnich B., Weiss A., 2002, A&A, 391, 195
González-García B. M., Zapatero Osorio M. R., Béjar V. J. S., Bihain G., Barrado Y Navascués D., Caballero J. A., Morales-Calderón M., 2006, A&A, 460, 799
Greisen E. W., Calabretta M. R., 2002, A&A, 395, 1061
Hambly N. C., Steele I. A., Hawkins M. R. S., Jameson R. F., 1995a, MNRAS, 273, 505
Hambly N. C., Steele I. A., Hawkins M. R. S., Jameson R. F., 1995b, A&AS, 109, 29
Hambly N. C. et al., 2008, MNRAS, 384, 637
Hawley S. L. et al., 2002, AJ, 123, 3409
Henry R. C., Anderson R., Hesser J. E., 1977, ApJ, 214, 742
Hewett P. C., Warren S. J., Leggett S. K., Hodgkin S. T., 2006, MNRAS, 367, 454
Hodgkin S. T., Irwin M. J., Hewett P. C., Warren S. J., 2009, MNRAS, 394, 675
Hogan E., Jameson R. F., Casewell S. L., Osbourne S. L., Hambly N. C., 2008, MNRAS, 388, 495
Jameson R. F., Casewell S. L., Bannister N. P., Lodieu N., Keresztes K., Dobbie P. D., Hodgkin S. T., 2008, MNRAS, 384, 1399
Jones B. F., Cudworth K., 1983, AJ, 88, 215
Kharchenko N. V., Piskunov A. E., Röser S., Schilbach E., Scholz R., 2005, A&A, 438, 1163
Klein-Wassink W. J., 1927, Groningen Publ. No. 41
Kraus A. L., Hillenbrand L. A., 2007, AJ, 134, 2340
Lawrence A. et al., 2007, MNRAS, 379, 1599
Lodieu N., Hambly N. C., Jameson R. F., Hodgkin S. T., Carraro G., Kendall T. R., 2007a, MNRAS, 374, 372
Lodieu N., Dobbie P. D., Deacon N. R., Hodgkin S. T., Hambly N. C., Jameson R. F., 2007b, MNRAS, 380, 712
Monet D. G. et al., 2003, AJ, 125, 984

Pinfield D. J., Hodgkin S. T., Jameson R. F., Cossburn M. R., von Hippel T., 1997, MNRAS, 287, 180
Pinfield D. J., Dobbie P. D., Jameson R. F., Steele I. A., Jones H. R. A., Katsiyannis A. C., 2003, MNRAS, 342, 1241
Sanders W. L., 1971, A&A, 14, 226
Skrutskie M. F. et al., 2006, AJ, 131, 1163
Tsvetkov T. G., 1993, Ap&SS, 203, 247
Vandenberg D. A., Bridges T. J., 1984, ApJ, 278, 679
van Leeuwen F., 2009, A&A, 497, 209
York D. G. et al., 2000, AJ, 120, 1579
Zacharias N., Urban S. E., Zacharias M. I., Wycoff G. L., Hall D. M., Monet D. G., Rafferty T. J., 2004, AJ, 127, 3043

APPENDIX A: SQL QUERIES

A1 UKIDSS–SDSS

```
SELECT
g.sourceID as u_id,
T2.slaveObjID as s_id,
g.ra as u_ra,
g.dec as u_dec,
T2.ra as s_ra,
T2.dec as s_dec,
m.mjdObs as u_mjd,
T2. mjd_z as s_mjd,
g.mergedClass as u_class,
g.zaperMag3 as u_z,
g.zaperMag3Err as u_zerr,
g.yaperMag3 as u_y ,
g.yaperMag3Err as u_yerr,
g.japerMag3 as u_j,
g.japerMag3Err as u_jerr,
g.haperMag3 as u_h,
g.haperMag3Err as u_herr,
g.k_1aperMag3 as u_k,
g.k_1aperMag3Err as u_kerr,
T2.psfMag_u as s_u,
T2.psfMagErr_u as s_uerr,
T2.psfMag_g as s_g,
T2.psfMagErr_g as s_gerr,
T2.psfMag_r as s_r,
T2.psfMagErr_r as s_rerr,
T2.psfMag_i as s_i,
T2.psfMagErr_i as s_ierr,
T2.psfMag_z as s_z,
T2.psfMagErr_z as s_zerr,

(T2.distanceMins * 60) as us_separation,

3.6e6*COS(RADIANS(g.dec))*(g.ra-T2.ra)/((m.mjdObs-T2.mjd_z)/365.25) AS us_pmra,
3.6e6*(g.dec-T2.dec)/((m.mjdObs-T2.mjd_z)/365.25) AS us_pmdec,

g.framesetid as framesetid,
f.multiframeid as multiframeid,
m.filename as filename,
m.catname as catname,
f.extNum as extnum,
T2.run as run,
T2.rerun as rerun,
T2.camcol as camcol,
T2.field as field,
T2.rowc_z as xpix,
T2.colc_z as ypix,
T2.segmentID as segmentID,
```

```
T2.stripe as stripe,
T2.chunkID as chunkID,
T2.startmu as startmu

FROM
gcsMergeLog as ml,
Multiframe as m,
gcsFrameSets as f,
  (
      SELECT sdss.ra, sdss.dec, x.slaveObjID, x.masterObjID, x.distanceMins,
      sdss.psfMag_u, sdss.psfMagErr_u, sdss.psfMag_g, sdss.psfMagErr_g, sdss.psfMag_r, sdss.psfMagErr_r,
      sdss.psfMag_i, sdss.psfMagErr_i, sdss.psfMag_z, sdss.psfMagErr_z, f.mjd_z, sdss.run, sdss.rerun,
      sdss.camcol, sdss.field, sdss.rowc, sdss.colc,sg.segmentID, sg.stripe, c.chunkID, c.startmu

      FROM gcsSourceXDR7PhotoObj as x, BestDR7..PhotoObj as sdss,
      BestDR7..Field as f, BestDR7..Segment as sg, BestDR7..Chunk as c

      WHERE sdss.type = 6 AND x.slaveObjID = sdss.objID AND f.fieldID = sdss.fieldID
      AND f.segmentID = sg.segmentID AND sg.chunkID = c.chunkID

        /* Detected in BINNED 1 */
        AND ((flags_i & 0x10000000) != 0)
        AND ((flags_z & 0x10000000) != 0)
        /* Not EDGE, NOPROFILE, PEAKCENTER, NOTCHECKED
        PSF_FLUX_INTERP, SATURATED, or BAD_COUNTS_ERROR */
        AND ((flags_i & 0x8100000c00a4) = 0)
        AND ((flags_z & 0x8100000c00a4) = 0)
        /* Not DEBLEND_NOPEAK or small PSF error */
        AND (((flags_i & 0x400000000000) = 0) or (psfmagerr_i <= 0.2))
        AND (((flags_z & 0x400000000000) = 0) or (psfmagerr_z <= 0.2))
        /* Not INTERP_CENTER or not COSMIC_RAY */
        AND (((flags_i & 0x100000000000) = 0) or (flags_i & 0x1000) = 0)
        AND (((flags_z & 0x100000000000) = 0) or (flags_z & 0x1000) = 0)

        AND distanceMins IN (
        SELECT MIN(distanceMins) FROM gcsSourceXDR7PhotoObj WHERE
        masterObjID = x.masterObjID AND distanceMins < 1.0 / 60
      )
  )

AS T2 RIGHT OUTER JOIN gcsSource AS g on g.sourceID=T2.masterObjID
WHERE
/* Sample selection predicates: Praesepe RA=120-150 deg && dec=15-25 deg */
g.ra BETWEEN 120.0 AND 135.0
AND g.dec BETWEEN 15.0 AND 25.0 and
(zXi BETWEEN −1.0 AND +1.0 OR zXi < −0.9e9)
AND yXi BETWEEN −1.0 AND +1.0
AND jXi BETWEEN −1.0 AND +1.0
AND hXi BETWEEN −1.0 AND +1.0
AND k_1Xi BETWEEN −1.0 AND +1.0
AND (zEta BETWEEN −1.0 AND +1.0 OR zEta < −0.9e9)
AND yEta BETWEEN −1.0 AND +1.0
AND jEta BETWEEN −1.0 AND +1.0
AND hEta BETWEEN −1.0 AND +1.0
AND k_1Eta BETWEEN −1.0 AND +1.0
AND (zClass BETWEEN −2 AND −1 OR zClass < −9999)
AND yClass BETWEEN −2 AND −1
AND jClass BETWEEN −2 AND −1
AND hClass BETWEEN −2 AND −1
AND k_1Class BETWEEN −2 AND −1
AND (priOrSec = 0 OR priOrSec = g.frameSetID)
AND g.frameSetID = ml.frameSetID
```

```
AND ml.zmfID = m.multiframeID
AND g.zppErrBits < 16
AND g.yppErrBits < 16
AND g.jppErrBits < 16
AND g.hppErrBits < 16
AND g.k_1ppErrBits < 16
AND g.framesetID=f.framesetID
AND f.multiframeID=m.multiframeID
```

A2 UKIDSS–2MASS

```
SELECT
g.sourceID as u_id,
T2.pts_key as t_id,
T2.designation t_designation,
g.ra as u_ra,
g.dec as u_dec,
T2.ra as t_ra,
T2.dec as t_dec,
m.mjdObs as u_mjd,
(T2.jdate-2400000.5) as t_mjd,
g.mergedClass as u_class,
g.zaperMag3 as u_z,
g.zaperMag3Err as u_zerr,
g.yaperMag3 as u_y,
g.yaperMag3Err as u_yerr,
g.japerMag3 as u_j,
g.japerMag3Err as u_jerr,
g.haperMag3 as u_h,
g.haperMag3Err as u_herr,
g.k_1aperMag3 as u_k,
g.k_1aperMag3Err as u_kerr,
T2.j_m as t_j,
T2.h_m as t_h,
T2.k_m as t_k,
T2.ph_qual as t_phqual,
T2.nopt_mchs as nopt_mchs,

(T2.distanceMins * 60) as ut_separation,

3.6e6*COS(RADIANS(g.dec))*(g.ra-T2.ra)/((m.mjdObs-(T2.jdate-2400000.5))/365.25) AS ut_pmra,
3.6e6*(g.dec-T2.dec)/((m.mjdObs-(T2.jdate-2400000.5))/365.25) AS ut_pmdec,

g.framesetid as framesetid,
f.multiframeid as multiframeid,
m.filename as filename,
m.catname as catname,
f.extNum as extnum

FROM
gcsMergeLog AS ml,
Multiframe AS m,
gcsFrameSets as f,

  (
      SELECT mass.designation, mass.pts_key, mass.ra, mass.dec, x.slaveObjID, x.masterObjID,
      x.distanceMins, mass.jdate, mass.j_m, mass.h_m, mass.k_m,
      mass.ph_qual,mass.nopt_mchs

      FROM gcsSourceXtwomass_psc AS x, TWOMASS..twomass_psc as mass
```

```
        WHERE x.slaveObjID = mass.pts_key AND mass.j_m > 9 AND mass.h_m > 8.5 AND mass.k_m > 8 AND
        distanceMins IN(
        SELECT MIN(distanceMins) FROM gcsSourceXtwomass_psc WHERE
        masterObjID = x.masterObjID AND distanceMins < 1.0 / 60
    )
  )
AS T2 RIGHT OUTER JOIN gcsSource AS g on g.sourceID=T2.masterObjID
WHERE
/* Sample selection predicates:Praesepe RA=120-135 deg && dec=15-25 deg */
g.ra BETWEEN 120.0 AND 135.0
AND g.dec BETWEEN 15.0 AND 25.0 and
(zXi BETWEEN −1.0 AND +1.0 OR zXi < −0.9e9)
AND yXi BETWEEN −1.0 AND +1.0
AND jXi BETWEEN −1.0 AND +1.0
AND hXi BETWEEN −1.0 AND +1.0
AND k_1Xi BETWEEN −1.0 AND +1.0
AND (zEta BETWEEN −1.0 AND +1.0 OR zEta < −0.9e9)
AND yEta BETWEEN −1.0 AND +1.0
AND jEta BETWEEN −1.0 AND +1.0
AND hEta BETWEEN −1.0 AND +1.0
AND k_1Eta BETWEEN −1.0 AND +1.0
AND (zClass BETWEEN −2 AND −1 OR zClass < −9999)
AND yClass BETWEEN −2 AND −1
AND jClass BETWEEN −2 AND −1
AND hClass BETWEEN −2 AND −1
AND k_1Class BETWEEN −2 AND −1
AND (priOrSec = 0 OR priOrSec = g.frameSetID)
AND g.frameSetID = ml.frameSetID
AND ml.zmfID = m.multiframeID
AND g.zppErrBits < 16
AND g.yppErrBits < 16
AND g.jppErrBits < 16
AND g.hppErrBits < 16
AND g.k_1ppErrBits < 16
AND g.framesetID=f.framesetID
AND f.multiframeID=m.multiframeID
```

APPENDIX B: HIGH PROBABILITY MEMBERS MATCHED TO PREVIOUS WORKS

Table B1. High probability members matched to previous works.

ID	Z	Y	J	H	K	μ_α (mas yr^{-1})	μ_δ (mas yr^{-1})	$P_{\rm mem}$ (per cent)	Previous IDs[a]
UGCS J083545.87+223042.	14.70	14.27	13.75	13.18	12.89	−35.9	−11.8	0.65	AD2057; KH561
UGCS J084207.83+221105.	14.84	14.39	13.84	13.27	12.99	−35.5	−7.3	0.76	AD3054; HSHJ406; KH691
UGCS J083722.41+220200.	14.11	13.61	13.05	12.52	12.21	−34.0	−4.2	0.77	AD2305; KH799
UGCS J084440.47+214553.	14.08	13.71	13.20	12.62	12.32	−34.6	−1.3	0.71	AD3337; KH508
UGCS J084120.88+215453.	13.96	13.71	13.24	12.64	12.43	−28.5	−10.4	0.75	AD2939
UGCS J084302.88+214513.	15.13	14.57	13.97	13.44	13.08	−29.6	−9.6	0.73	AD3161; KH989
UGCS J083256.66+213829.	15.82	15.43	14.92	14.36	14.05	−38.2	−6.3	0.69	AD1687
UGCS J084126.00+213425.	15.93	15.42	14.82	14.31	13.94	−36.7	−3.8	0.72	AD2951; HSHJ367; KH901
UGCS J084458.84+213217.	15.64	15.28	14.76	14.28	13.98	−27.8	−0.6	0.61	AD3361
UGCS J083454.93+213854.	15.19	14.75	14.17	13.59	13.28	−34.2	−1.4	0.71	AD1951; KH773
UGCS J083526.81+213901.	15.74	15.25	14.65	14.10	13.77	−37.8	−8.8	0.68	AD2021; KH843
UGCS J083912.55+213557.	15.90	15.43	14.81	14.24	13.93	−29.2	−7.2	0.75	AD2517; HSHJ250
UGCS J083413.87+212352.	15.25	14.75	14.18	13.61	13.31	−27.8	−8.1	0.71	AD1868; KH786
UGCS J083434.27+212207.	14.54	14.06	13.46	12.89	12.59	−29.2	−5.2	0.75	AD1915; KH681

Table B1 – *continued*

ID	Z	Y	J	H	K	μ_α (mas yr^{-1})	μ_δ (mas yr^{-1})	$P_{\rm mem}$ (per cent)	Previous IDs[a]
UGCS J083316.62+212020.	14.08	13.64	13.11	12.54	12.26	−29.8	−9.3	0.74	AD1737; KH677
UGCS J084143.40+212950.	15.93	15.25	14.60	14.08	13.70	−31.7	−12.4	0.67	AD3006; HSHJ386; KH1084
UGCS J084030.70+212333.	14.94	14.56	14.04	13.47	13.19	−29.1	−9.0	0.73	AD2776; HSHJ318;
UGCS J084048.51+212949.	13.64	13.43	13.00	12.40	12.24	−26.0	−8.8	0.81	AD2828
UGCS J082935.64+212047.	14.79	14.53	14.07	13.45	13.26	−31.2	−4.2	0.77	AD1252
UGCS J084536.22+211521.	13.74	13.38	12.87	12.28	12.01	−26.8	−1.4	0.73	AD3427; HSHJ497; JS604; KH450
UGCS J084457.00+210648.	15.58	15.11	14.54	13.97	13.67	−28.3	−6.2	0.73	AD3358; KH835
UGCS J083813.89+210926.	13.91	13.55	13.07	12.47	12.21	−31.8	−9.9	0.63	HSHJ198; JS216; KH453
UGCS J083459.25+210837.	15.42	14.84	14.24	13.69	13.37	−32.9	−1.7	0.73	AD1962; KH961
UGCS J084123.94+211519.	15.62	15.24	14.73	14.17	13.90	−28.4	−3.9	0.72	AD2945
UGCS J084719.06+211102.	15.58	15.11	14.51	13.95	13.64	−25.2	−6.3	0.60	KH814
UGCS J084711.92+210748.	15.72	15.22	14.60	14.07	13.74	−32.4	−12.3	0.67	HSHJ501; KH926
UGCS J083730.73+210740.	14.94	14.51	13.99	13.42	13.13	−32.7	−9.7	0.75	KH564
UGCS J082927.94+210838.	13.39	13.11	12.65	12.04	11.80	−31.1	−3.6	0.78	AD1240; KH397
UGCS J084515.55+210335.	14.41	14.04	13.52	12.96	12.69	−36.0	−1.9	0.70	AD3394; HSHJ496; KH574
UGCS J084620.04+210032.	15.80	15.29	14.69	14.14	13.82	−36.7	−6.4	0.73	AD3506; HSHJ499; KH927
UGCS J084321.75+205510.	15.07	14.78	14.28	13.74	13.48	−26.7	−4.8	0.67	AD3195
UGCS J082942.64+205707.	14.03	13.78	13.28	12.70	12.48	−28.4	−0.3	0.61	AD1263
UGCS J083629.41+210310.	14.94	14.54	14.01	13.44	13.16	−31.7	−13.5	0.61	AD2175; HSHJ125; KH614
UGCS J083715.24+205759.	14.20	13.90	13.42	12.82	12.59	−27.5	−2.5	0.66	AD2291
UGCS J083401.54+210039.	15.77	15.27	14.67	14.11	13.80	−25.4	−5.6	0.61	AD1837; KH871
UGCS J084114.43+205946.	15.63	15.17	14.58	14.02	13.71	−30.7	−1.0	0.70	AD2918; HSHJ356; KH838
UGCS J084859.88+204155.	15.69	15.12	14.50	13.99	13.62	−39.3	−6.6	0.63	KH965
UGCS J083918.03+204421.	13.67	13.36	12.86	12.26	12.05	−31.6	−8.5	0.74	AD2538; JS284; KH419
UGCS J083922.13+204758.	15.27	14.78	14.20	13.65	13.32	−32.3	−4.5	0.78	AD2551; HSHJ261; KH828
UGCS J083232.42+205040.	14.45	14.06	13.53	12.95	12.70	−26.5	−5.8	0.67	AD1632; JS10; KH528
UGCS J083845.67+203943.	15.44	15.02	14.43	13.90	13.60	−34.5	−4.1	0.77	AD2452; KH812
UGCS J083615.51+204109.	13.15	12.90	12.44	11.83	11.62	−31.7	−4.8	0.78	AD2138; JS117; KH357
UGCS J083603.23+205015.	15.67	15.18	14.61	14.08	13.74	−33.6	−5.7	0.78	AD2101; HSHJ096; KH841
UGCS J084114.04+204429.	13.97	13.53	12.96	12.38	12.12	−26.5	−5.2	0.87	AD2916; JS416; KH707
UGCS J083711.87+204047.	14.03	13.72	13.20	12.59	12.35	−27.7	−11.9	0.61	AD2284; JS166l; KH477
UGCS J083406.67+204946.	15.71	15.26	14.68	14.11	13.80	−29.4	−5.6	0.76	AD1852; KH818
UGCS J084418.23+204948.	15.45	14.94	14.32	13.76	13.46	−38.4	−1.7	0.61	AD3300; HSHJ478
UGCS J083300.38+204310.	13.72	13.35	12.79	12.23	11.95	−32.0	−3.9	0.73	AD1699; JS19; KH706
UGCS J083804.60+203935.	14.95	14.53	13.95	13.38	13.08	−33.0	−10.4	0.74	KH663; JS704;
UGCS J084849.96+202635.	13.44	13.15	12.66	12.07	11.81	−28.7	−4.3	0.86	KH392
UGCS J085032.50+203419.	14.27	13.97	13.51	12.99	12.81	−34.0	−0.3	0.68	AD3783
UGCS J084545.87+202940.	13.78	13.44	12.92	12.34	12.09	−28.4	−8.8	0.83	AD3447; JS609; KH460
UGCS J084047.77+202847.	14.03	13.61	13.09	12.49	12.25	−33.6	−7.9	0.78	AD2825; KH554
UGCS J083314.23+203621.	15.71	15.20	14.57	14.03	13.72	−28.5	−8.4	0.72	AD1731; KH892
UGCS J083808.16+202646.	13.70	13.35	12.82	12.22	12.01	−30.8	−6.5	0.83	KH418
UGCS J084611.69+203800.	14.36	14.04	13.50	12.99	12.71	−32.2	−6.8	0.79	AD3490
UGCS J083338.36+202852.	15.31	14.82	14.25	13.71	13.43	−27.1	−10.7	0.62	AD1786; KH724
UGCS J083943.59+202939.	14.54	14.14	13.60	13.03	12.75	−25.7	−5.7	0.63	AD2618; JS311; KH629
UGCS J083912.08+203607.	14.84	14.38	13.82	13.27	12.96	−39.3	−6.0	0.64	AD2515
UGCS J083903.93+203402.	13.98	13.60	13.07	12.50	12.24	−25.8	−7.4	0.84	AD2502; JS266; KH500
UGCS J082750.59+201436.	12.50	12.26	11.85	11.32	11.09	−26.0	−0.4	0.60	AD1025; KH300
UGCS J084111.05+202238.	13.44	13.12	12.63	12.04	11.81	−25.7	−5.8	0.85	AD2905; JS411; KH416
UGCS J084137.35+201236.	15.15	14.66	14.09	13.56	13.27	−30.2	−1.2	0.69	AD2988; HSHJ381; KH667
UGCS J083641.16+201639.	15.04	14.60	13.98	13.45	13.14	−30.7	−5.6	0.78	AD2205; KH693
UGCS J083642.16+201622.	15.46	14.97	14.37	13.85	13.52	−32.3	−9.9	0.75	AD2208
UGCS J084423.19+201355.	15.34	14.84	14.28	13.72	13.42	−29.1	−4.8	0.75	AD3312; KH787
UGCS J083041.51+202426.	15.55	15.17	14.68	14.10	13.84	−37.2	−9.0	0.69	AD1396
UGCS J083311.09+201604.	15.16	14.74	14.17	13.67	13.37	−31.8	−12.6	0.66	AD1719
UGCS J083942.01+201745.	14.98	14.50	13.93	13.39	13.11	−31.5	−0.8	0.70	AD2615; KH808
UGCS J083906.87+202054.	13.54	13.23	12.75	12.14	11.94	−25.1	−5.5	0.83	AD2508; JS270; KH426
UGCS J083507.87+202023.	14.46	14.07	13.55	12.99	12.71	−30.9	−9.5	0.75	AD1978; KH496
UGCS J083436.75+201155.	13.71	13.41	12.93	12.32	12.08	−30.4	−6.4	0.84	AD1921; HSHJ058; JS63
UGCS J084151.90+202047.	13.85	13.51	13.00	12.41	12.18	−29.9	−8.4	0.82	AD3026; JS459; KH470
UGCS J083855.15+201308.	14.31	13.90	13.35	12.77	12.50	−32.3	0.1	0.67	AD2478; HSHJ234; JS255; KH606

Table B1 – *continued*

ID	Z	Y	J	H	K	μ_α (mas yr^{-1})	μ_δ (mas yr^{-1})	$P_{\rm mem}$ (per cent)	Previous IDs[a]
UGCS J083825.35+202120.	15.93	15.45	14.85	14.32	13.99	−31.1	−11.8	0.69	KH903
UGCS J083539.26+202409.	14.98	14.48	13.88	13.35	13.04	−31.4	−8.2	0.77	AD2042; KH854
UGCS J085237.29+200043.	13.46	13.26	12.84	12.27	12.13	−26.4	−5.0	0.86	AD4003
UGCS J083259.56+200714.	15.87	15.39	14.81	14.27	13.93	−33.9	−12.6	0.65	AD1696; KH896
UGCS J084332.60+195932.	14.73	14.31	13.75	13.19	12.88	−34.2	−3.9	0.77	AD3211; HSHJ458; KH655
UGCS J083333.93+200425.	14.27	13.89	13.36	12.76	12.52	−26.6	−6.4	0.67	AD1774; HSHJ043; KH509
UGCS J083559.43+200440.	14.87	14.41	13.81	13.26	12.95	−36.5	−1.0	0.66	AD2091; HSHJ091; JS687; KH743
UGCS J083622.40+200706.	15.36	14.89	14.32	13.76	13.45	−26.3	−7.9	0.65	AD2155; KH774
UGCS J084034.83+194937.	14.85	14.52	14.04	13.46	13.19	−34.7	−5.9	0.77	AD2790
UGCS J083608.58+195725.	15.13	14.65	14.05	13.49	13.19	−26.1	−9.0	0.62	AD2115; HSHJ102; KH884
UGCS J083619.14+195354.	14.34	13.94	13.41	12.82	12.56	−31.4	−8.2	0.77	AD2147; HSHJ115; JS123; KH593
UGCS J083707.63+195727.	15.47	14.99	14.43	13.87	13.56	−32.5	−7.8	0.78	AD2275; KH864
UGCS J083727.87+195412.	14.32	13.91	13.38	12.78	12.53	−32.7	−11.3	0.71	AD2328; KH638
UGCS J084030.57+195558.	14.15	13.76	13.25	12.64	12.42	−27.0	−10.5	0.63	AD2775; HSHJ320; JS356; KH546
UGCS J084801.27+194939.	15.40	14.95	14.37	13.79	13.50	−32.5	−5.6	0.79	KH727
UGCS J084823.56+195011.	14.64	14.23	13.65	13.07	12.78	−31.9	1.1	0.62	KH579
UGCS J085056.86+193657.	14.44	14.05	13.52	12.93	12.67	−30.7	0.6	0.63	KH527
UGCS J082757.39+191130.	15.94	15.55	14.98	14.37	14.12	−36.2	−9.1	0.72	AD1043
UGCS J083439.68+190812.	14.61	14.18	13.63	13.05	12.78	−32.7	−4.5	0.78	AD1925; HSHJ060; KH596
UGCS J083430.71+190600.	14.46	14.08	13.53	12.96	12.73	−38.2	−9.9	0.63	AD1906; HSHJ055; JS675; KH513
UGCS J082848.63+185835.	15.82	15.26	14.63	14.07	13.72	−31.5	−5.9	0.78	AD1164; KH1025
UGCS J083150.86+185902.	15.29	14.85	14.32	13.79	13.47	−29.9	0.6	0.62	AD1549
UGCS J083218.87+190308.	14.64	14.21	13.64	13.08	12.78	−33.6	−8.4	0.77	AD1607; HSHJ023; KH594
UGCS J083544.59+185738.	15.40	14.93	14.35	13.80	13.50	−29.2	−6.0	0.75	AD2053; HSHJ084; KH858
UGCS J083651.05+190418.	14.99	14.61	14.09	13.51	13.22	−28.7	−4.4	0.73	AD2231; HSHJ136; KH565
UGCS J083305.56+185548.	13.93	13.55	13.01	12.43	12.17	−22.8	−4.3	0.66	AD1707; JS22; KH519
UGCS J083338.00+185717.	14.21	13.86	13.31	12.74	12.49	−38.5	−7.4	0.67	AD1785; HSHJ045; JS41; KH482
UGCS J083051.38+185351.	15.25	14.81	14.22	13.66	13.38	−32.3	0.0	0.67	AD1411; HSHJ008; KH670
UGCS J083734.95+185607.	14.47	14.11	13.60	13.09	12.84	−32.2	−6.9	0.79	HSHJ173
UGCS J083235.23+184409.	15.94	15.41	14.79	14.24	13.95	−27.6	−6.1	0.71	AD1641; HSHJ024
UGCS J083207.94+184426.	14.37	13.97	13.47	12.87	12.59	−26.9	−1.6	0.61	AD1588; KH511
UGCS J083154.25+184536.	15.59	15.08	14.51	13.96	13.64	−28.9	−5.9	0.75	AD1555; HSHJ018; KH834
UGCS J083126.88+184056.	15.41	14.84	14.19	13.64	13.30	−29.9	−6.8	0.77	AD1500; KH1044
UGCS J083658.63+184952.	15.19	14.63	14.04	13.51	13.17	−28.2	−7.6	0.72	AD2248; KH923
UGCS J083808.07+184429.	15.80	15.28	14.68	14.11	13.82	−27.0	−10.5	0.63	HSHJ196; KH779
UGCS J083729.39+184135.	14.89	14.48	13.94	13.38	13.10	−37.7	−7.2	0.70	HSHJ165; KH542
UGCS J083528.37+184032.	15.73	15.21	14.63	14.10	13.76	−27.3	−3.6	0.68	AD2022
UGCS J083506.21+184924.	14.76	14.33	13.77	13.20	12.92	−38.7	−3.8	0.64	AD1975; HSHJ068; JS680; KH644
UGCS J083540.13+184228.	14.15	13.72	13.18	12.62	12.33	−34.2	−5.9	0.78	AD2045; HSHJ082; JS95; KH636
UGCS J083434.30+184756.	14.13	13.73	13.19	12.62	12.37	−32.5	−12.6	0.66	AD1917; HSHJ056; JS62; KH570
UGCS J083343.93+184750.	14.31	13.90	13.40	12.81	12.54	−31.9	−13.7	0.60	AD1797; HSHJ047; JS44; KH526
UGCS J083328.19+184336.	15.96	15.40	14.81	14.28	13.95	−38.4	−4.3	0.67	AD1763; HSHJ041; KH874
UGCS J083142.95+182906.	15.26	14.81	14.22	13.64	13.36	−26.2	−7.9	0.65	AD1532; HSHJ017; KH699
UGCS J083140.88+182942.	14.89	14.47	13.90	13.34	13.08	−32.9	−5.7	0.79	AD1526; HSHJ016; KH563
UGCS J083521.67+182934.	13.98	13.59	13.11	12.53	12.28	−27.0	−7.6	0.86	AD2011; HSHJ076; JS87; KH463
UGCS J083334.78+183108.	13.24	12.97	12.54	11.98	11.84	−26.6	−3.3	0.83	AD1776; JS40
UGCS J083014.08+182519.	14.56	14.15	13.61	13.08	12.78	−35.1	−11.9	0.66	AD1344; HSHJ004; KH559
UGCS J083453.83+180105.	15.72	15.23	14.61	14.05	13.73	−32.0	−10.9	0.72	AD1948; HSHJ065; KH817
UGCS J083547.20+180829.	14.54	14.12	13.52	12.94	12.67	−30.7	−11.7	0.69	AD2063; HSHJ087; KH628
UGCS J083002.92+175702.	15.79	15.24	14.65	14.07	13.72	−32.0	−12.0	0.69	AD1308; HSHJ002; KH990
UGCS J083517.03+173624.	15.12	14.59	14.00	13.43	13.14	−27.1	−7.7	0.68	AD2000; HSHJ074; KH855
UGCS J083839.13+172948.	15.98	15.49	14.88	14.33	14.02	−30.6	−10.7	0.72	AD2436; HSHJ217; KH904
UGCS J084026.64+172100.	14.82	14.48	13.98	13.40	13.13	−29.9	−2.9	0.73	AD2760
UGCS J083855.64+171509.	14.51	14.12	13.56	12.99	12.70	−27.4	−2.3	0.65	AD2482; KH608
UGCS J083824.87+165836.	14.09	13.71	13.16	12.59	12.31	−32.8	−2.0	0.74	AD2396; KH478
UGCS J083906.50+170100.	14.58	14.06	13.51	12.96	12.64	−36.2	−7.5	0.74	AD2507
UGCS J083608.51+165717.	13.88	13.54	13.05	12.50	12.22	−29.8	−4.0	0.84	AD2114

[a]AD – Adams et al. (2002), HSHJ – Hambly et al. (1995b), JS – Jones & Cudworth (1983) and KH – Kraus & Hillenbrand (2007).

APPENDIX C: NEW HIGH PROBABILITY MEMBERS

Table C1. New high probability members.

ID	Z	Y	J	H	K	μ_α (mas yr^{-1})	μ_δ (mas yr^{-1})	$P_{\rm mem}$
UGCS J083925.46+214721.9	15.46	15.12	14.62	14.06	13.81	−31.1	−8.8	0.76
UGCS J083301.71+213902.1	13.95	13.75	13.35	12.73	12.58	−24.6	−4.5	0.80
UGCS J084826.25+213235.7	15.98	15.59	15.02	14.48	14.20	−32.4	−1.6	0.73
UGCS J083310.88+210959.8	13.38	13.15	12.71	12.10	11.92	−22.9	−6.5	0.70
UGCS J083032.17+211015.4	15.26	14.96	14.46	13.84	13.66	−29.4	−7.3	0.76
UGCS J083956.01+211419.1	15.84	15.49	15.00	14.43	14.18	−25.5	−4.8	0.61
UGCS J083553.75+191055.8	15.11	14.85	14.39	13.79	13.61	−26.2	−6.3	0.65
UGCS J083115.62+184708.9	15.89	15.58	15.13	14.57	14.35	−31.1	−0.3	0.68
UGCS J083448.26+181300.2	14.46	14.26	13.82	13.21	13.08	−27.6	−4.5	0.70
UGCS J083459.25+181805.4	15.43	15.19	14.71	14.10	13.88	−32.9	−1.5	0.72
UGCS J083306.96+174242.1	15.29	14.77	14.16	13.61	13.31	−26.3	−3.6	0.63
UGCS J083701.06+172005.1	14.80	14.47	13.94	13.41	13.12	−28.1	−7.2	0.72
UGCS J084709.34+172925.6	15.45	15.11	14.58	14.12	13.87	−33.1	−9.3	0.76
UGCS J083455.71+170918.5	13.90	13.72	13.30	12.70	12.56	−22.6	−4.1	0.63

APPENDIX D: SDSS CANDIDATE MEMBERS

Table D1. SDSS–UKIDSS selected candidates.

ID	Z	Y	J	H	K	μ_α (mas yr^{-1})	μ_δ (mas yr^{-1})	Prob	Fit order[a]
UGCS J084218.27+212342.1	18.18	17.50	16.81	16.27	15.88	−4.05	−6.32	0.00	12
UGCS J084804.97+211515.1	19.64	18.57	17.68	17.05	16.59	67.66	64.70	0.00	6
UGCS J084346.46+210829.4	18.46	17.68	17.00	16.45	16.06	−28.38	−38.64	0.00	12
UGCS J084956.26+205300.0	17.88	17.30	16.65	16.09	15.71	32.59	−53.01	0.00	12
UGCS J082924.86+211700.3	16.10	15.59	15.02	14.57	14.27	−94.95	−133.65	0.00	12
UGCS J084138.84+211655.5	17.88	17.29	16.55	16.03	15.72	9.02	20.03	0.00	12
UGCS J084449.14+210153.6	18.77	17.79	16.95	16.41	15.94	0.36	23.91	0.00	12
UGCS J084507.41+210056.5	18.69	17.87	17.06	16.49	16.14	−36.74	−40.16	0.00	12
UGCS J084204.64+205941.1	16.77	16.09	15.42	14.93	14.54	114.67	−167.13	0.00	12
UGCS J082839.58+205401.5	18.48	17.69	16.91	16.34	15.95	15.24	−31.20	0.00	12
UGCS J082945.32+205455.0	19.26	18.48	17.67	17.10	16.51	4.16	−22.41	0.00	12
UGCS J083054.47+190119.4	16.13	15.47	14.76	14.21	13.84	−15.32	−128.89	0.00	12
UGCS J084433.77+214430.7	17.77	17.01	16.30	15.74	15.32	−37.33	32.77	0.00	6
UGCS J084650.44+214805.4	17.37	16.68	16.08	15.62	15.28	−75.34	−117.60	0.00	12
UGCS J083301.71+213534.7	18.65	17.93	17.20	16.61	16.17	14.87	18.57	0.00	6
UGCS J084306.24+214134.2	18.40	17.56	16.71	16.16	15.73	−38.63	−44.50	0.00	12
UGCS J083141.80+183500.4	15.65	15.07	14.45	13.98	13.64	46.31	−110.20	0.00	12
UGCS J083353.37+182609.4	19.20	18.17	17.24	16.64	16.18	6.73	−8.95	0.00	12
UGCS J083955.10+222300.8	19.06	18.11	17.27	16.64	16.21	−11.29	−9.27	0.58	12
UGCS J083110.12+181252.7	18.15	17.48	16.74	16.20	15.75	38.81	−45.95	0.00	12
UGCS J083654.60+195415.7	18.75	17.96	17.10	16.53	15.96	−26.97	28.33	0.00	12
UGCS J083648.03+194902.2	18.21	17.34	16.55	15.97	15.52	−98.98	−17.63	0.00	6
UGCS J084714.47+194643.8	18.06	17.45	16.80	16.27	15.86	14.68	6.35	0.00	12
UGCS J085052.56+195321.9	19.24	18.34	17.40	16.75	16.22	−5.74	−21.30	0.00	12
UGCS J084652.65+172017.9	18.67	17.91	17.15	16.62	16.18	16.12	−30.63	0.00	12
UGCS J084045.71+171218.3	19.09	18.17	17.20	16.60	16.17	−33.60	1.04	0.58	12
UGCS J084452.78+171409.8	18.77	17.76	16.90	16.33	15.84	−44.67	−13.78	0.00	12
UGCS J083900.61+204356.2	20.05	18.76	17.91	17.33	16.72	2.62	−71.34	0.00	12
UGCS J083920.28+204629.5	19.34	18.49	17.65	16.95	16.51	−5.94	−12.50	0.00	12
UGCS J083721.24+204306.1	19.73	18.66	17.56	16.84	16.33	25.55	9.35	0.00	12
UGCS J083737.24+202902.6	19.71	18.60	17.39	16.64	16.04	−34.02	−61.35	0.00	12
UGCS J083019.80+203418.8	18.95	17.92	17.11	16.59	16.13	−10.23	−93.17	0.00	12
UGCS J083724.09+164812.9	18.55	17.81	17.10	16.53	16.10	−5.67	11.58	0.00	12

Table D1 – *continued*

ID	Z	Y	J	H	K	μ_α (mas yr^{-1})	μ_δ (mas yr^{-1})	Prob	Fit order[a]
UGCS J083954.96+202955.7	18.90	17.91	17.06	16.44	15.98	33.38	−54.56	0.00	12
UGCS J084926.31+202127.0	18.64	17.76	17.00	16.54	16.08	−75.67	−30.17	0.00	12
UGCS J085002.02+201725.9	19.28	18.56	17.64	17.05	16.53	−44.04	50.96	0.00	12
UGCS J083203.66+202035.8	19.90	18.68	17.74	17.04	16.52	−31.90	−59.39	0.00	12
UGCS J083531.32+201838.9	18.39	17.62	16.96	16.39	15.99	−17.01	20.43	0.00	12
UGCS J083748.01+201448.5	18.09	17.25	16.51	15.94	15.53	−36.17	−44.57	0.00	12

[a]For some objects not enough reference stars could be found to perform the quadratic fit. In this case the fit was reduced to a linear one (six free parameters) as indicated in the fit order column.

This paper has been typeset from a TEX/LATEX file prepared by the author.